University of Groningen

Deep GMOS spectroscopy of extremely red galaxies in GOODS-South

Roche, Nathan D.; Dunlop, James; Caputi, Karina I.; McLure, Ross; Willott, Chris J.; Crampton, David

Link to publication in University of Groningen/UMCG research database

Deep GMOS spectroscopy of extremely red galaxies in GOODS-South: ellipticals, mergers and red spirals at $1 < z < 2$

Nathan D. Roche,[1]⋆† James Dunlop,[1]† Karina I. Caputi,[2]† Ross McLure,[1]† Chris J. Willott[3]† and David Crampton[3]†

[1]*Institute for Astronomy, University of Edinburgh, Royal Observatory, Blackford Hill, Edinburgh EH9 3HJ*
[2]*Institut d'Astrophysique Spatiale, bat.121 – Universite Paris, XI 91405 Orsay Cedex, France*
[3]*Herzberg Institute of Astrophysics, National Research Council, 5071 West Saanich Road, Victoria, BC, Canada V9E 2E7*

ABSTRACT

We have performed a deep (35.5-h exposure) spectroscopic survey of extremely red ($I - K > 4$) galaxies (ERGs) on the Great Observatories Origins Deep Survey (GOODS)-South Field, using the Gemini multi-object spectrograph on the 8-m Gemini South Telescope. We present here spectra and redshifts for 16 ERGs at $0.87 < z < 2.02$, to a limit of $K_s \simeq 20.2$. In the spectra of 10 of these galaxies we find emission lines of [O II] 3727 Å with fluxes corresponding to a mean star formation rate (uncorrected for dust) of $1.6\,M_\odot\,\mathrm{yr}^{-1}$. For three ERGs we detect no emission lines and the remaining three lie at $z > 1.5$ where this line would be outside our wavelength range. Absorption features are seen in most ERG spectra.

We examine the morphologies of these ERGs on *Hubble Space Telescope* Advanced Camera for Surveys (*HST*-ACS) images and fit radii and Sersic indices. We find three broad classes: (i) spheroidals; (ii) mergers at a variety of stages (some are spheroidal–disc pairs, some have tidal tails), often with a high surface brightness and (iii) red spirals (which may have star forming regions in their outer discs).

We perform an age-dating analysis by fitting the spectra and nine-band photometry (*BVIZJHK*, plus 3.6/4.5-μm fluxes from Spitzer) of the ERGs with two-component models, consisting of passively evolving, old stellar populations combined with a younger, continuously star forming component, for which the age and dust extinction are allowed to vary from 10 to 800 Myr and $E(B - V) = 0.0$ to 0.5 mag. For only one ERG is the best-fitting model purely passive, for the others the best fit is obtained by including a star forming component, which typically forms a few (0.26–13.5) per cent of the stellar mass, and is subject to dust reddening averaging $E(B - V) \simeq 0.35$. The ages of the star forming components tend to be youngest (10–40 Myr) in the merging ERGs, and older (200–800 Myr) in spiral ERGs, with mixed ages for the spheroidals.

The best-fitting mean ages for the old stellar populations range from 0.6 to 4.5 Gyr, averaging 2.1 Gyr, with masses from 3×10^{10} to $2 \times 10^{11}\,M_\odot$. The mean stellar formation redshifts of ERGs are spread from $\sim$0.5 Gyr before the epoch of observation out to $z \sim 5$. We propose that most ERGs are galaxies, or mergers of galaxies, formed some Gyr earlier, in an early ($z \sim 5$) phase of massive galaxy formation, which since then have experienced a wide variety of merger and star formation (SF) histories, accounting for the wide range of observed stellar ages.

Finally, we examine the clustering of the ERGs on this field, as a function of the photometric redshifts estimated by Caputi et al. The comoving correlation radius is $r_0 \simeq 13\,h^{-1}$ Mpc for the full sample and, dividing by redshift, is constant or increasing with redshift, thus favouring comoving ($\epsilon = -1.2$) evolution over a stable ($\epsilon = 0$) clustering model.

⋆Present address: Astronomy and Cosmology Research Unit, University of KwaZulu-Natal, Durban 4041, South Africa.
†E-mails: roche@ukzn.ac.za (NDR); jsd@roe.ac.uk (JD); kcaputi@ias.u-psud.fr (KIC); rjm@roe.ac.uk (RM); chris.willott@nrc.ca (CJW); david.crampton@nrc.ca (DC)

1 INTRODUCTION

The 'extremely red galaxies' (ERGs, also known as EROs) are a population of faint and distant galaxies, appearing in large numbers faintward of $K \sim 18$, with very red optical/near-infrared (IR) colours ($R - K > 5$ or $I - K > 4$), corresponding to galaxies which are already old and passively evolving at $z > 1$. The ERGs are of great importance in understanding galaxy evolution, in particular they represent an evolutionary link between the rapidly star forming galaxies detected by SCUBA at $z > 2$, and present-day massive E/S0 galaxies.

A key property of ERGs is their strong clustering, as revealed by measurements of their angular correlation function, $\omega(\theta)$ (e.g. Daddi et al. 2000; Firth et al. 2002; Roche et al. 2002; Roche, Dunlop & Almaini 2003). Assuming a comoving model of clustering evolution, these observations give for ERGs a correlation radius $r_0 \simeq 10$–$13\,h^{-1}$ Mpc (where $h = H_0/100\,\mathrm{km\,s^{-1}\,Mpc^{-1}}$), which supports their interpretation as the progenitors of giant ellipticals.

However, ERGs are actually a very diverse population of galaxies. Spectroscopic observations find that some are indeed old, passive galaxies at $z > 1$ (e.g. Dunlop et al. 1996); however, at least half of the ERGs show emission lines (Cimatti et al. 2002; Yan, Thompson & Soifer 2004a) indicating ongoing SF. X-ray (Daddi et al. 2004) and mid-IR (Yan et al. 2004b) observations indicate that many emission-line ERGs are actually undergoing major starbursts, with SF rates (SFRs) as high as $\sim$50–100 $M_\odot$ yr^{-1}. Secondly, deep X-ray surveys reveal at least $\sim$10 per cent of ERGs to host an obscured active galactic nucleus (AGN) (Alexander et al. 2002; Roche et al. 2003). Thirdly, ERGs are morphologically diverse; a mixture of bulges, discs, irregulars and mergers (e.g. Cimatti et al. 2003; Yan & Thompson 2003).

Initially, we (Roche et al. 2002) colour-selected a sample of 158 ERGs with $K \leqslant 21$ on the ELAIS N2 field. We found evidence of strong clustering and a mixture of morphologies, and identified seven ERGs as radio sources (either AGN or powerful starbursts). We also fitted the ERG number counts with a model in which they evolve into the present-day E/S0 population, through a combination of passive luminosity evolution, merging and a gradual increase with time in the comoving number density of red galaxies.

For our second study (Roche et al. 2003, hereafter RDA03), deeper optical *Hubble Space Telescope* Advanced Camera for Surveys (*HST*-ACS) and near-IR (NIR) [Very Large Telescope (VLT)-ISAAC] data enabled us to colour-select 198 ERGs to a fainter limit of $K = 22$, on a central region of the *Chandra*/Great Observatories Origins Deep Survey (GOODS) Deep Field South. For the clustering of these ERGs we estimated $r_0 = 12.5 \pm 1.2\,h^{-1}$ Mpc, and we identified 17 ERGs with X-ray sources in the 1-Ms *Chandra* survey (Giacconi et al. 2002), from the X-ray fluxes diagnosing 13 as obscured AGN and the other four as probable starbursts.

In our third study, Caputi et al. (2004) fitted template spectra to the seven-band optical/NIR photometry of these same ERGs to derive photometric redshift estimates, which in turn were used to estimate stellar masses and luminosity functions. Caputi et al. (2005) then extended this analysis to the full sample of $K < 22$ galaxies on this field (see Section 6).

In this paper, we further investigate the CDFS ERGs by means of a deep optical spectroscopic survey, with the Gemini multi-object spectrograph (GMOS). We aim to measure redshifts and emission lines for a sample of ERGs to a limit $K_s = 20$–21, and furthermore to estimate the ages of these galaxies by fitting evolving models to their spectra and broad-band fluxes (including new 3.6-/4.5-μm fluxes from Spitzer). We shall interpret and discuss these results and make comparisons with the photometrically based analysis of Caputi et al. (2004, 2005) and the recent spectrographic surveys of ERGs presented by Yan et al. (2004a), McCarthy et al. (2004), Daddi et al. (2004, 2005), Doherty et al. (2005) and Longhetti et al. (2005).

In Section 2 of this paper, we describe the optical/NIR data from RDA03 and our new GMOS observations, and in Section 3 the reduction and calibration of the spectroscopic data. In Section 4, we present spectra for the ERGs where we have secure or probable redshifts, fit models to estimate ages and masses, and measure emission-line fluxes. In Section 5, we describe the morphology of the ERGs and estimate their size and surface brightness. In Section 6, we re-examine the clustering of the RDA03 ERGs as a function of spectroscopic and photometric redshift, and in Section 7 conclude with interpretation and discussion.

Throughout this paper the assumed cosmology is $\Omega_m = 0.25$, $\Omega_\Lambda = 0.75$, and $H_0 = 70\,\mathrm{km\,s^{-1}\,Mpc^{-1}}$, in accord with the recent (3-yr *Wilkinson Microwave Anisotropy Probe*) estimates of Spergel et al. (2006). This gives the age of the Universe as 14.16 Gyr. Magnitudes are given in the Vega system except where labelled by subscript as *AB* magnitudes, the conversion between the two being $(K_s, H, J, I_{775})_{AB} = (K_s, H, J, I_{775})_{\mathrm{Vega}} + (1.841, 1.373, 0.904, 0.403)$.

2 OBSERVATIONS

2.1 Optical/NIR imaging

The *Chandra* Deep Field South forms one of the two fields of the publicly available European Southern Observatories (ESO) GOODS. As an early part of GOODS, deep imaging in the NIR H, J and K_s bands was obtained for a central region of the CDFS, covering 50.4 arcmin^2 and centred at right ascension (RA) $3^{\mathrm{h}}\,32^{\mathrm{m}}\,30^{\mathrm{s}}$, declination (Dec.) $-27°\,48'\,30''$ (equinox 2000.0), using the ISAAC camera on the 'Antu' VLT (at the ESO site at Cerro Paranal, Chile). Also as part of GOODS, the central CDFS was mapped in four bands ($B_{435}\ V_{606}\ I_{775}\ Z_{850}$) with the *HST*-ACS (Giavalisco et al. 2004). Most recently, the GOODS Field South is currently being surveyed with Spitzer at 3.6–24 μm. For this paper, we have available 3.6- and 4.5-μm fluxes for the galaxies on this field, derived from the 'epoch 2' data release of 2005 May.

First, to define our ERG sample, we ran the source detection program SEXTRACTOR on the mosaiced ISAAC K_s-band data, to obtain a sample of $K_s \leqslant 22$ galaxies (with completeness limit $K_s \simeq 21.5$). For more details of this, see RDA03. With SEXTRACTOR we measured for these galaxies both total and aperture (2.0 arcsec diameter circular) magnitudes.

These $K_s \leqslant 22$ galaxies were positionally matched to the corresponding detections on the ISAAC H and J mosaics and the ACS I_{775} images. Colours were measured for each as the differences in the 2.0 arcsec aperture magnitudes, and the ERG sample was then selected as the $K_s < 22$ galaxies redder than $I_{775} - K_s = 3.92$, which
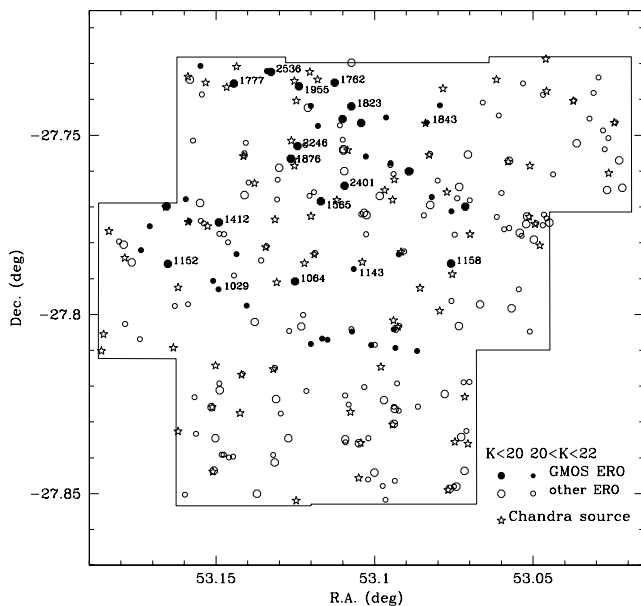
numbered 198 in the 50.4 arcmin^2 area. We numbered these objects 1–2555 using their order of detection in the $K_s < 22$ catalogue.

For the galaxies studied in this paper we also measure 3.6- and 4.5-μm fluxes from the Spitzer 'epoch 2' data release of 2005 May. The Spitzer data have a lower resolution of full width at half-maximum (FWHM) $\simeq 1.6$ arcsec. Because of this, larger apertures of 2.8 arcsec diameter were employed to measure the Spitzer fluxes, and to these fluxes aperture corrections of 0.5 mag for 3.6 μm and 0.55 mag for 4.5 μm were applied, as derived from the point spread function (PSF).

2.2 Spectroscopic observations

The target galaxies for our GMOS survey form a subset of the RDA03 sample, consisting primarily of the brighter, $K_s < 21$, ERGs within a 5.5×5.5 arcmin^2 area that can be covered by a single GMOS mask. A spectrograph mask was prepared with 47 slitlets (each of length 2.0 arcsec and width 1.0 arcsec) devoted to our target ERGs. Fig. 1 shows their positions within the larger area of our CDFS sample. Observations were performed with GMOS on the Gemini South telescope in Chile, over the period from 2003 September 24 to 2004 February 21, using the low-dispersion, R150 grating and central wavelengths in the region of 7500 Å. In total we were able to obtain 70 exposures, totalling 35.5 h, through the ERG slit mask. These science observations were interspersed with CuAr arc lamp and standard star exposures, for wavelength and flux calibration.

These observations utilized GMOS in the 'nod-and-shuffle' mode described in detail by Abraham et al. (2004). The sky background is a serious problem for ground-based spectroscopy, especially at redder, $\lambda > 7500$ Å wavelengths where there are strong emission lines. The 'nod-and-shuffle' mode was designed to provide improved subtraction of the sky background, even where this is subject to considerable spatial and time variation. Essentially, the telescope is 'nodded' (by 1 arcsec in this case) along the spectroscopic slit, observing at each

position alternately in a rapid one-minute cycle. In position A the object will be towards one side of the slit and the adjacent sky on the other, in position B the object will be on the other side. With each cycle, the charges stored on the CCD from the two positions are 'shuffled' (by 2 arcsec) into adjacent strips on the CCD frame, where they are accumulated over the course of each half-hour exposure. In this way the sky is observed simultaneously with, and as close as possible in position to, each individual target galaxy.

3 DATA REDUCTION

GMOS data reduction was carried out using IRAF routines, including some specifically written for this instrument. First, bias frames were subtracted from the target galaxy, arc lamp and standard star exposures. The next step was sky subtraction, performed individually for each of the 70 exposures. The nod-and-shuffle mode produces a CCD frame showing two adjacent strips for each spectrograph slit, corresponding to the two nod positions. To sky subtract, the frame is shifted by the shuffle step and subtracted it from itself (using the IRAF 'gnsskysub' task). This produces a positive and a negative sky-subtracted spectrum for each target galaxy.

Small dithers in the spectral and spatial directions between the 70 exposures (introduced intentionally for the removal of charge traps; Abraham et al. 2004) were removed by registering the 70 exposures in both axes. The 70 sky-subtracted frames could then be combined, using IRAF 'imcombine' with a 'sigclip' rejection to remove most of the cosmic rays, into a single 35.5-h image, from which we extract the spectra.

IRAF tasks (e.g. 'apall') were then employed to extract the 2D spectra from each slit, summing each in the spatial direction to give a 1D spectrum. With nod and shuffle it is necessary to extract both the positive and a negative spectrum for each object, and then subtract one from the other.

The galaxy spectra were wavelength calibrated using the CuAr lamp calibration spectrum as observed through the same slit of the mask. Each pixel is approximately 3.5 Å and the resolution of our spectra FWHM $\simeq 18$ Å. Flux calibration was performed using a co-added spectrum of the calibration standard star LTT1020, and the spectral energy distribution of this star as tabulated by Hamuy et al. (1994), to derive (using IRAF 'sensfunc') a sensitivity function for the spectrograph (Fig. 2a).
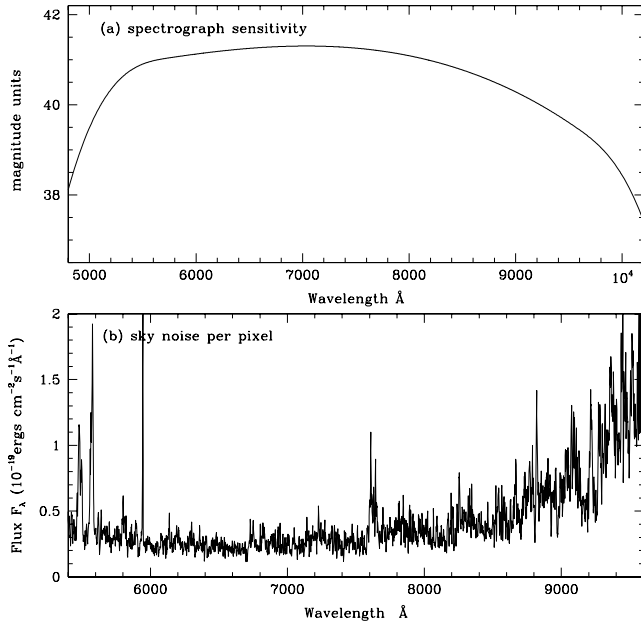
Corrections were also applied to the spectra for the telluric (Earth's atmosphere) absorption bands, using our calibration spectrum of a white dwarf standard star (these having few intrinsic spectral features), EG131. This was divided by a fit to its own continuum, giving a function almost flat at unity except for four telluric absorption bands, centred at 6560, 6875, 7610 and 9075 Å. These were extracted, converted into magnitude units, and inserted into a function $y(\lambda) = 1$ to give a telluric correction function.

The ERG spectra were divided by this correction function and by the sensitivity function, to give spectra calibrated in F_ν (in units of 10^{-29} erg cm^{-2} s^{-1} Hz^{-1}, i.e. μJy), and F_λ (in units 10^{-19} erg cm^{-2} s^{-1} Å^{-1}), ready for further analysis.

4 SPECTRA OF THE ERGS

4.1 Defining the redshift sample

On examining the GMOS spectra we found that our survey had a good rate of success for ERGs to $K_s \simeq 20$, but failed to reach the fainter $K_s = 21$ limit of the target list. Of our 47 spectra of ERG targets, 16 were galaxy spectra of sufficient quality that we were

Figure 1. Positions of the 198 ERGs in the CDFS sample of RDA03, within the borders of its 50.4 arcmin^2 area. The *Chandra* X-ray sources (Giacconi et al. 2002) are also shown. Bold symbols indicate the 47 ERGs targeted by our GMOS spectroscopic survey, and the 16 of these which form our redshift sample (see Section 3 and Table 1) are labelled with their ID numbers.

Figure 2. (a) Sensitivity of the spectrograph as a function of wavelength (as measured using calibration star LTT1020) and (b) sky noise within an extracted spectrum, calibrated in F_λ.

able to determine good or, at least, likely redshifts. 17 showed no significant signal, 13 had some signal in the continuum but we were unable to confidently identify any spectral features above the noise, and one was identified as a red Galactic star. The 16 'successful' spectra include 13 of the 18 target ERGs with $K_s < 20$, three of the six target ERGs with $20 < K_s < 20.25$ but none fainter than this.

Redshifts were estimated by a combination of (i) fitting models to the continuum, by the method described below, (ii) identifying absorption features and (iii) from emission lines such as [O II] 3727 Å where present. For galaxies with an emission line we determine both an emission (z_{em}) and a continuum-fit/absorption-line (z_{cf}) redshift. In all cases we found the two consistent within the $\sim 0.01z$ statistical error on z_{cf}. Where both are given z_{em} is likely to be more precise.

Two of these redshifts, for the galaxies 1843 and 1158, are based on spectral features of poor signal-to-noise ratio and must be regarded as less reliable than the other 14. However, these two redshifts are supported by good fits of our model spectra to the photometry.

We therefore define a redshift sample comprised of these 16 ERGs. The 16 redshifts range from $z = 0.868$ to 2.017, with six in a 'spike' at $1.180 \leqslant z \leqslant 1.225$, which may be indicative of large-scale structure. One of the 16 ERGs, ID no. 1843, corresponds to a *Chandra* source. This is XID:253 in the list of Giacconi et al. (2002), with a flux and hardness ratio (HR $= 0.66 \pm 0.11$) indicative of an obscured AGN (see RDA03).

4.2 Comparison with spectroscopy of other authors

Some of the objects in our redshift sample were recently observed spectroscopically by other authors, in separate and independent studies, published during the writing of this paper – Vanzella et al. (2005), who used FORS2 on the VLT, and Doherty et al. (2005), using DEIMOS on Keck. For objects in the overlap between these surveys, we make a brief comparison of the spectra.

(i) Our object 1152 is in Vanzella et al. (2005) as GDS J033239.64−274709.1. The FORS2 spectrum gave $z = 1.317$, consistent with our $z = 1.309$, and similarly shows weak [O II] emission, and absorption lines. 1152 is also object 2800 in Doherty et al. (2005), observed with DEIMOS giving $z = 1.318$, with H & K absorption. Neither spectrum goes far enough into the red to see well the Balmer lines.

(ii) Object 1029 was observed as GDS J033235.79−274734.7. The FORS2 spectrum gave $z = 1.223$, consistent with our $z = 1.221$, and is very similar to ours, with strong [O II] emission and some absorption features, including (weak) Balmer lines.

(iii) Object 1412 is GDS J033235.78−274627.5. The FORS2 spectrum gave $z = 1.094$, consistent with our $z = 1.092$, and like ours shows [O II] emission. The H8 and H9 lines we find are not identified on the FORS2 spectrum, but it extends further into the red to reveal Hγ and Hδ absorption. Thus, on the basis of both spectra this seems to be a strong Balmer absorption galaxy.

(iv) Object 1777 was not observed in the FORS2 survey.

(v) Object 2536 is GDS J033231.83−274356.2. The FORS2 spectrum gave $z = 1.550$, slightly higher than our $z = 1.513$. Like our GMOS spectrum it features MgII (2800 Å) absorption, and extends a little further redwards, detecting an [O II] emission line.

(vi) Object 1064 is GDS J033230.02−274726.8. The FORS2 spectrum gave $z = 1.553$, a close match to our $z = 1.548$, and detects MgII (2800 Å) absorption, and a weak [O II] emission line at the reddest extreme.

(vii/viii/ix) Objects 1143 and 1565 and 2401 were not observed in the FORS2 survey.

(x) Object 1876 is GDS J033230.34−274523.6. The FORS2 spectrum gave $z = 1.223$, slightly higher than our $z = 1.196$. The FORS2 spectrum, like ours, shows MgII (2800 Å) absorption, [O II] emission and Balmer lines, extending further redwards to Hγ. 1876 is also number 2158 in the Doherty et al. (2005) DEIMOS sample, where it has $z = 1.222$ and H& K, Hδ absorption, very weak [O II], and is classed as E+e.

(xi) Object 2246 is GDS J033229.82−274510.8. The FORS2 spectrum gave $z = 1.225$, slightly greater than our $z = 1.196$. Like our spectrum it shows [O II] emission and H& K absorption, the spectra are very similar but ours has better signal-to-noise ratio.

(xii/xiii) Objects 1823 and 1955 were not observed in the FORS2 survey.

(xiv) Object 1762 is GDS J033227.02−274407.2. The FORS2 spectrum gave $z = 1.127$, slightly higher than our $z = 1.102$, and like ours shows moderate [O II] emission and weak Balmer absorption. The authors mark Hγ but it is barely visible.

(xv) Objects 1843 and 1158 were not observed in the FORS2 survey. However, the AGN 1843 was observed with VLT FORS in an earlier survey of *Chandra* sources. Szokoly et al. (2004) initially proposed $z = 0.484$ on the basis of a single unidentified line. Zheng et al. (2004) claimed $z = 1.89$ on the basis of a single line, this time supported by photometric redshifts from COMBO-17 and hyper-z. However, for our nine-band photometry we obtain a hyper-z solution of $z = 2.06$, and our continuum is significantly better fitted for $z = 2.017$ than $z = 1.89$. Considering that photometric redshifts are uncertain by at least 8 per cent, we retain $z = 2.017$ as a provisional and approximate estimate. NIR spectroscopy should detect multiple emission lines and give an unambiguous answer.

In summary, out of our redshift sample of 16, eight objects were also observed by Vanzella et al. (2005) and/or Doherty et al. (2005), who obtained very similar spectra similar spectra (although in two cases with a redshift discrepancy that might be larger than expected

from statistical error). Seven of our redshifts appear to be new. Finally, for the $z \sim 2$ AGN, more data are needed.

4.3 Model fitting

We fit our ERG spectra, at $5800 < \lambda < 9000\,\text{Å}$ where the signal-to-noise ratio is the greatest, with a series of 40 template spectra from Jimenez et al. (2004). These represent passively evolving stellar populations, with a Salpeter initial mass function and solar metallicity, at ages from 0.001 to 14 Gyr. We experimented with models of lower and higher metallicity but found no indication that these fitted any better. Furthermore, the colours (Caputi et al. 2004) of our ERGs and the ultraviolet (UV) spectroscopy of de Mello et al. (2004) support the assumption that ERGs have approximately solar metallicity, even to $z \sim 2$.

From the scatter between the 17 'blank' (i.e. no signal) slit spectra, we derived a function representing the noise per pixel produced by the sky background within the area of a single spectroscopic slit (Fig. 2b). This is much worse at the red end due to strong sky emission lines and the declining detector response.

We fit models to a combination of the GMOS spectra and the nine-band ($BVIZJHK$, 3.6/4.5 μm) photometry, using a least-squares (minimum χ^2) method, with each pixel of the spectrum weighted using this noise function. The GMOS spectrum and the nine-band photometry make similar contributions to the combined χ^2, which is minimized in the fitting.

An initial series of fits as a function of redshift provided the continuum-fit redshift z_{cf} for each ERG. We then fixed the redshift at this value and fit with a *two-component* model, this being the sum of a single-age passively evolving model, of age T_{pas}, and a 'starburst' component of much younger stars, represented by the model of Jimenez et al. (2004), integrated with a constant SFR for a time interval T_{sb} prior to the time of observation. It is important to note that this component is not a single-age population, but contains stars of all ages from zero to T_{sb}. The young component is subject to dust reddening, following the extinction curve of Calzetti et al. (2000), parametrized in terms of $E(B - V)$. The normalization of the young component is parametrized as f_{sb} the fraction of the emitted flux it contributes in the rest-frame B band, 4500 Å. Hence it is described by three parameters, T_{sb}, $E(B - V)$ and f_{sb}.

For each ERG, we searched for the best-fitting model, by calculating a χ^2 for the GMOS spectrum, plus the nine-band photometry compared with a set of model spectra, forming a grid of 18 000 points in the 4D ($T_{pas}, f_{sb}, T_{sb}, E(B - V)$) parameter space. T_{sb} was allowed to vary from 10 to 800 Myr and $E(B - V)$ from 0 to 0.5 mag ($A_V \sim 2$ mag). The best-fitting model was taken as the position within this grid where χ^2 has the minimum value χ^2_{min}.

Error intervals were estimated for the fitted parameters, as follows. Using our grid of models and their associated χ^2, we find the surface in parameter space, enclosing the best-fitting model, on which χ^2 takes the value $\chi^2_{min} + 2.71$ (χ^2_{min}/N_{df}), where N_{df} is the number of degrees of freedom, approximately 900 here. This surface defines an approximately 90 per cent confidence interval. The error on a given parameter, e.g. T_{pas}, is then taken as the *projection* of this entire surface on to the T_{pas} axis (*not* just its intercept with the axis). This projected interval will then take into account any degeneracies between the fitted parameters, which would produce an elongated surface and hence widen the projected error interval.

The models of Jimenez et al. (2004) are normalized in units of solar masses and so the normalizations of the model fits can provide estimates of the stellar mass in each galaxy, for both the passive (M_{pas}) and the young (M_{sb}) stellar components. However, the model

fits to the nine-band aperture photometry always gave higher normalizations than fits to the spectra (by factors of 1.1–2.5), the reason being that a 2.0 arcsec diameter aperture admits a greater fraction of the light from an extended galaxy than the 1.0 arcsec spectrograph slit. We therefore give stellar mass estimates with the higher normalization given by fitting models to the aperture photometry.

4.4 Spectra and ages of the redshift sample

Fig. 3 shows plots of our 16 GMOS spectra, the nine-band photometry and best-fitting models. Spectra and models are normalized to fit the aperture (rather than slit) photometry.

Table 1 lists coordinates of the 16 galaxies and Table 2 the best-fitting parameters T_{pas}, M_{pas}, M_{sb} and f_{sb}, with approximately 90 per cent confidence interval error bars. Also given are a flux-weighted mean SF redshift, z_{msf}, which corresponds to the look-back time T_{pas} earlier than the redshift of observation, the masses of the passive and starburst components in the best-fitting model, plus Mf_{sb} [$= M_{sb}/(M_{pas} + M_{sb})$] the fraction of the total stellar mass in the starburst/young component. Table 3 gives the nine-band aperture photometry, absolute magnitude M_B (AB system) in the rest-frame B band, derived from the best-fitting model normalized to the 2.0 arcsec aperture magnitudes, and M_{BT} an absolute magnitude with an approximate correction to total magnitude given by adding the (small) difference between aperture and total K magnitudes.

We find a wide variation in T_{pas} within the sample, from 0.6 to 4.5 Gyr, with a mean of 2.1 ± 0.3 Gyr, and in the mass M_{pas}, from $3 \times 10^{10}\,\text{M}_\odot$ to almost $2 \times 10^{11}\,\text{M}_\odot$, with a mean $1.1 \times 10^{11}\,\text{M}_\odot$. Note that we have performed two independent reductions of the GMOS data, and the other reduction was independently fit with both the models given by Jimenez et al. (2004) and Bruzual & Charlot (2003). These analyses gave age estimates closely similar to, and consistent with, those presented here.

Only for one ERG was the best fit obtained for a purely passive model, $f_{sb} = 0$. For the 15 where χ^2 is smaller with $f_{sb} > 0$, the best-fitting star forming component made up anything from 0.26 to 13.5 per cent of the total stellar mass (mean 3.5 ± 1.1 per cent). The best-fitting ages and dust reddenings for the star forming components vary widely between individual ERGs, and cover the full range allowed in this model, 10–800 Myr (mean 364 ± 96 Myr) and 0–0.5 mag (mean 0.35 ± 0.05).

For six ERGs, the best-fitting star forming component is a short-term, <100 Myr starburst, always with some dust reddening varying from $E(B - V) = 0.2$ to 0.5. For nine others, the best fit is with a longer period (100–800 Myr) of continuous SF, in three cases with little/no dust but in the other six with heavy extinction of $E(B - V) \simeq 0.5$. In Section 7.3, we discuss how age and recent SF history is related to morphology.

4.5 Spectral lines

10 of the 16 ERG spectra show a single emission line, which in all cases is assumed to be [O II] 3727 Å. In most cases, this identification is supported by the position of other spectral features. [O II] 3727 Å emission is an indicator of ongoing or very recent (within $\sim 10^7$ yr) SF, and according to Kennicutt (1998), a luminosity $L_{O\,II}$ erg s^{-1} in this line corresponds to a SFR $1.4 \times 10^{-41}\,L_{O\,II}\,\text{M}_\odot\,\text{yr}^{-1}$.

For three ERGs we find no emission at 3727 Å indicating that SF has ceased, is at a very low level, and/or is heavily obscured. One of these (2401) has a spectrum fit by a purely passive model, but the photometry of the other two (1701 and 1955) is best fit with the inclusion of a heavily reddened young component, suggesting these
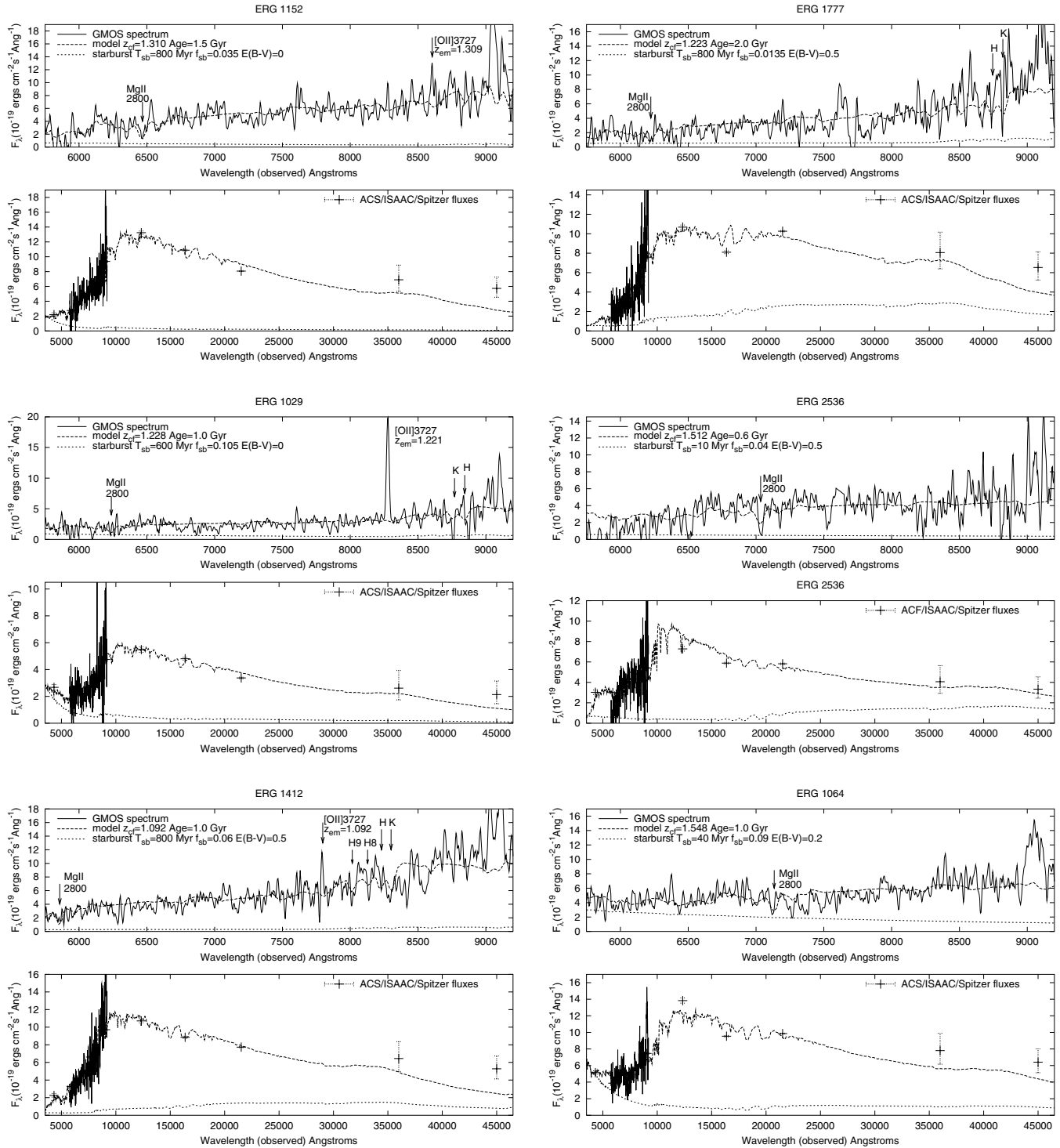
Figure 3. GMOS spectra and broad-band (ACS/ISAAC/Spitzer) photometry of 16 ERGs, calibrated in F_λ. For each the upper plot shows the GMOS spectrum (solid line), our best-fitting two-component model (dotted), and, where non-zero, the starburst component of the model. Labelled are the age of the model passive component, and the time-scale T_{sb}, fractional flux contribution at $\lambda_{rest} = 4500$ Å, f_{sb} and dust reddening $E(B-V)$ of the starburst component, and obvious spectral features. The lower plot shows a wider wavelength range with the nine broad-band fluxes, the GMOS spectrum (solid) and the best-fitting models as in the upper plot. Both plots are normalized to the 2.0-arcsec aperture fluxes.

are dusty post-starbursts. Three ERGs lie at $z > 1.5$ where [O II] would not be visible in our wavelength range, but two of these have [O II] visible at the red extreme of the FORS2 spectra (which have a slightly redder limit), and all three have strong fluxes at the blue end.

Absorption features are prominent in almost all ERG spectra, the Mg II close doublet at 2800 Å and/or H & K (3934, 3968 Å), and the ~4000 Å break is generally a prominent feature, indicating the presence of old stellar populations. Three emission-line ERGs (1412, 1823, 1876) show H8 and H9 Balmer
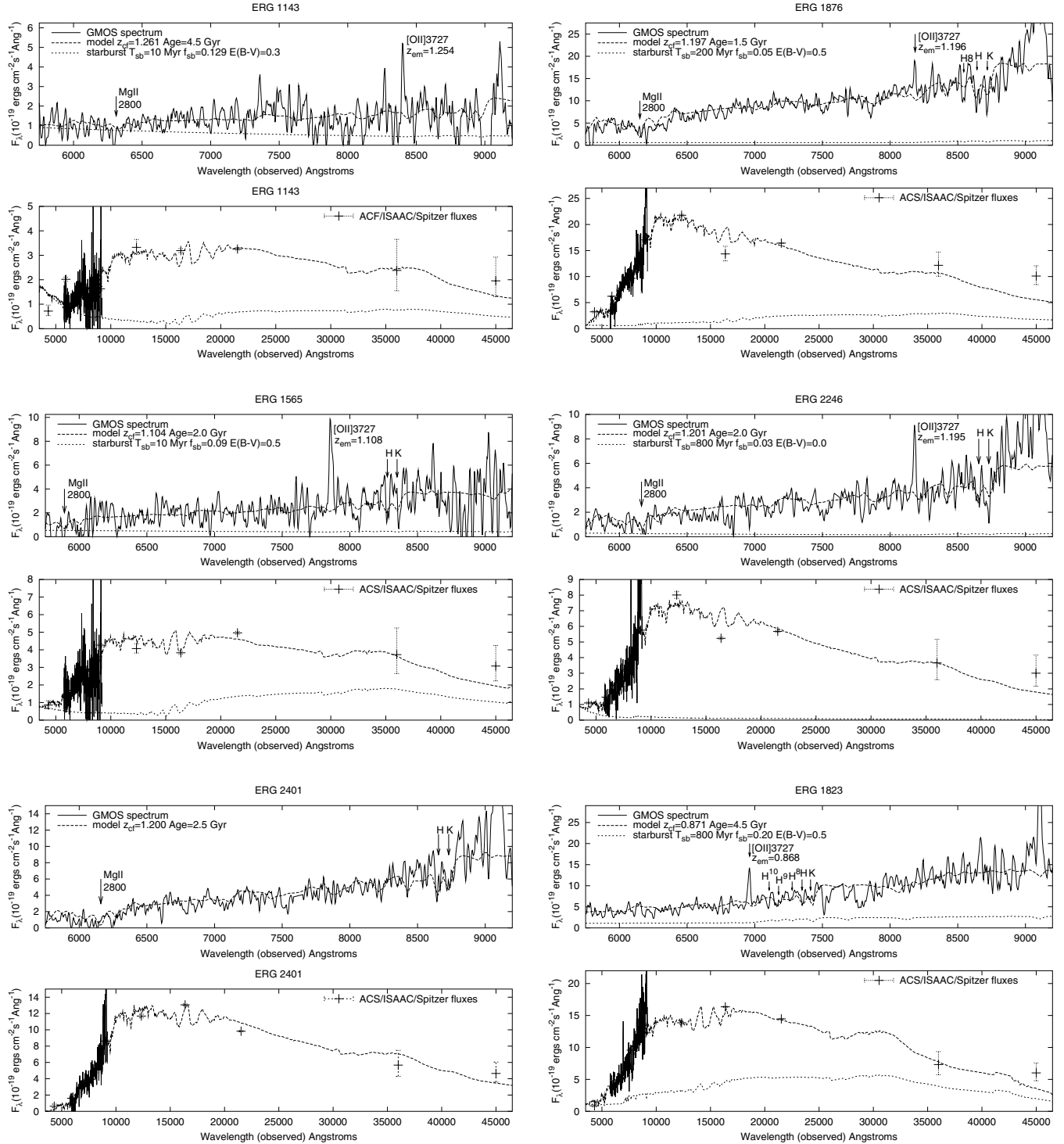
Figure 3 – continued.

absorption lines indicating a large intermediate-age (10^8–10^9 yr) component.

The [O II] 3727 Å line fluxes were measured from the GMOS spectra (using IRAF 'splot'), and multiplied by the ratio of the continuum flux in the 2.0 arcsec aperture to that in the GMOS slit, so as to obtain a line flux more representative of the entire galaxy. The [O II] line fluxes are listed in Table 4, with errors calculated by summing the sky noise function (Fig. 2b) over the resolution element

(18 Å) centred on the observed line wavelength. From this flux and the spectroscopic redshift we derive the [O II] 3727 Å luminosity of the galaxy, which is uncorrected for dust, and from this SFR $_{O II}$, using the relation of Kennicutt (1998).

These SFRs, which again are uncorrected for dust extinction, average $1.61 \pm 0.37\,M_\odot\,\mathrm{yr}^{-1}$. There are two ways in which we can estimate a very approximate dust-corrected SFR. First, if the emission lines are assumed to be subject to the same dust extinction
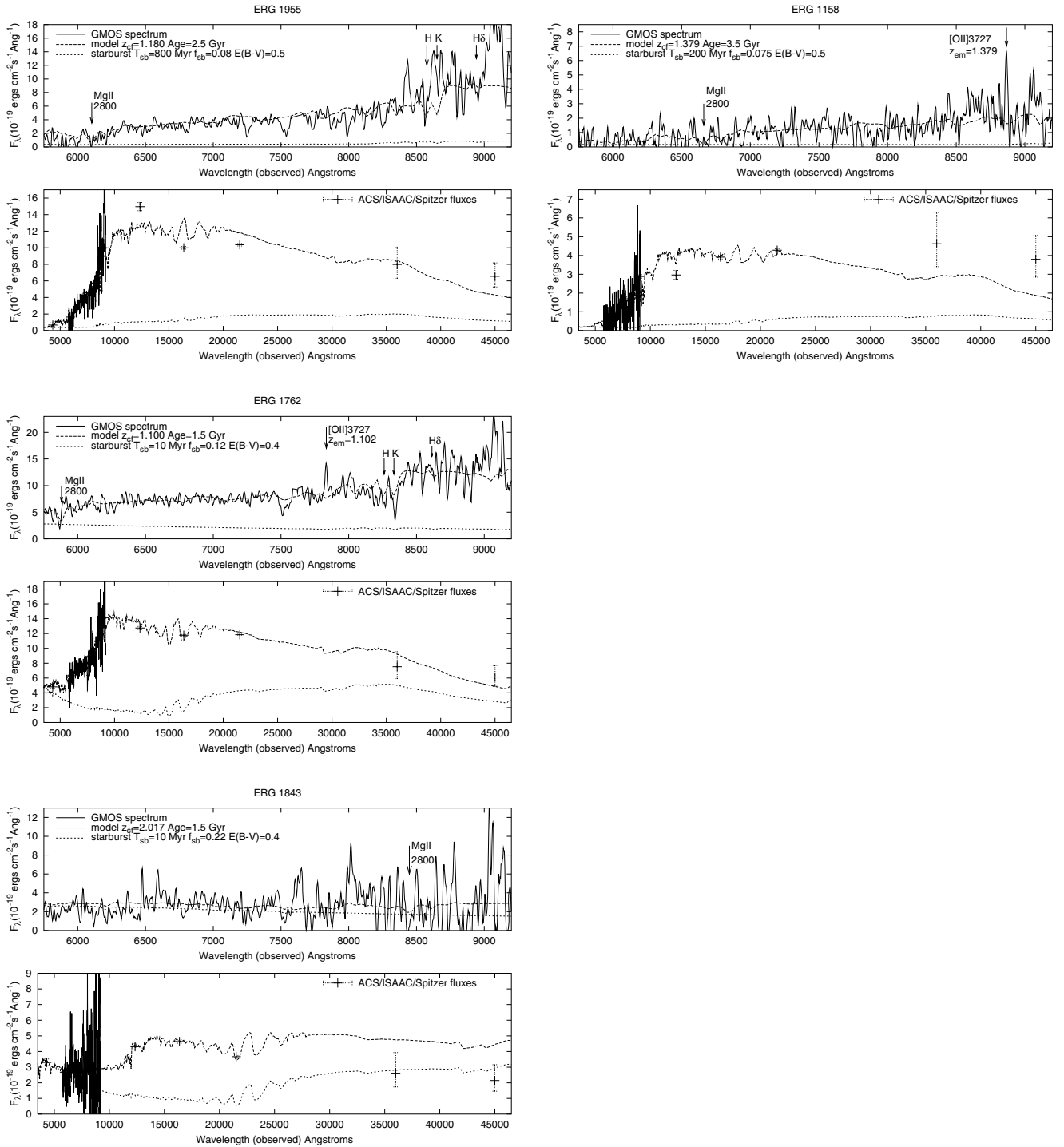
Figure 3 – continued.

as the continuum, then from the reddening curve of Calzetti et al. (2000) the [O II] extinction is found to be $A_{3727} = 5.86E(B - V)$. If we apply this correction to the SFRs in Table 4, using the value of $E(B - V)$ best fit to the spectrum of each galaxy, the mean SFR of the 10 emission-line galaxies increases to $12.6\,\mathrm{M_\odot\,yr^{-1}}$.

Secondly, if we assume that the SFR and dust extinction in the star forming component is truly constant, we can estimate $\mathrm{SFR_{sb}} = M_{sb}/T_{sb}$. This will correct for dust, as this is taken into account in calculating M_{sb}, but for an individual ERG this is very approximate

due to the large error bars on T_{sb}. For the full sample of ERGs (but excluding the AGN), the mean $\mathrm{SFR_{sb}}$ is $24\,\mathrm{M_\odot\,yr^{-1}}$.

5 MORPHOLOGY AND SIZE OF ERGS IN THE REDSHIFT SAMPLE

The *HST*-ACS images, in the stacked form used here (version V1.0 from the STScI), have a pixel size 0.03 arcsec and resolution FWHM $\simeq 0.08$ arcsec ($\simeq 0.66$ kpc at $z = 1.2$). Fig. 4 shows all 16 galaxies as

Table 1. RA and Dec. coordinates of the 16 ERGs in our redshift sample; and total K magnitude (Vega system).

ID no.	RA (°)	Dec. (°)	K_{total}
1152	53.165 199	−27.785 870	19.14
1029	53.149 200	−27.792 976	20.21
1412	53.149 109	−27.774 279	19.23
1777	53.144 367	−27.735 580	18.87
2536	53.132 652	−27.732 313	19.60
1064	53.125 080	−27.790 777	18.98
1143	53.106 606	−27.787 319	20.23
1565	53.116 936	−27.768 448	19.77
2401	53.109 440	−27.764 095	18.93
1876	53.126 465	−27.756 538	18.24
2246	53.124 275	−27.752 996	19.68
1823	53.107 304	−27.741 930	18.61
1762	53.112 560	−27.735 302	18.66
1955	53.123 837	−27.736 311	18.91
1843	53.083 546	−27.746 445	20.00
1158	53.075 893	−27.785 822	19.78

they appear on the I_{775}-band ACS image, and Fig. 5 the B_{435}-band images ($\lambda_{rest\,frame} \sim 2000$ Å), which have poorer signal-to-noise ratio but provide extra information by highlighting regions of SF.

The appearance of each ERG is described briefly below (by 'high-SB' we mean an I_{775}-band central surface brightness of about 0.033 counts pixel^{-1} s^{-1} = 21.7 AB mag arcsec^{-2}, a value typical of the spheroidal ERGs).

1152 ([O II] emitter) is a high-SB spheroidal surrounded by a much fainter ring (post-merger?). Only the central nucleus is visible in the B image.

1029 ([O II] emitter) appears in I to be a normal spheroidal, with a bulge profile. However, the B image shows spots within the galaxy which could be SF regions.

1412 ([O II] emitter) is a large ($\sim$1.8 arcsec diameter) disc with spiral arms and a small central nucleus. In B the nucleus cannot be seen but two brighter regions in the outer arms are just visible.

1777 (no [O II]) is a barred spiral of large diameter ($\sim$2.4 arcsec) and relatively low SB. A nucleus and two spiral arms are clearly visible in I. It does not appear disturbed. In the B image, the nucleus and arms cannot be seen and all that is visible is a tiny bright spot within the N spiral arm.

2536 ($z > 1.5$; UV-bright) is a merging pair of separation $\sim$0.25 arcsec. The NW component is smaller but higher in SB, the SE is irregular with bright regions on the W and SE sides. In the B band both galaxies are visible, but only the W and SE parts of the irregular component and the centre of the NW galaxy are prominent. Both galaxies appear to contain bright SF regions within redder discs/spheroids. This ERG has the youngest T_{pas} of our sample combined with a young ongoing starburst.

1064 ($z > 1.5$; UV-bright) appears in the I band to be a high-SB elliptical. However, in the B band the nucleus disappears and is replaced by bright regions on either side of it, forming a bar. This bar is very asymmetric and there is no sign of spiral arms, implying that this galaxy is not a barred spiral but a merger.

1143 ([O II] emitter) is a very small spheroidal, without visible features (in both I and B) but appears to be a dusty starburst.

1565 ([O II] emitter) is a complex system, with four separate intensity peaks. The southernmost galaxy has the highest SB in I and could be a spheroid. Only one of the four components, an amor-

phous galaxy at the NW, is visible in B. This could be a multiple merger of a star forming and three passive galaxies.

2401 (no [O II]) is a small, roundish, high-SB spheroid. It is extremely faint in the B band. The spectrum gives no evidence of ongoing or recent SF.

1876 ([O II] emitter) appears to be a large, face-on spiral with a high-SB nucleus, and two arms reaching to a radius $\simeq 0.9$ arcsec. The galaxy is ringed by bright regions, presumably star forming hotspots on the basis of their visibility in the B image, with gaps in the ring at the N and S. This galaxy has a strong colour gradient; the nucleus ($r < 0.5$ arcsec) has a 'passive' colour of $(B - I)_{AB} = 2.49$, but the ring ($0.5 < r < 1.2$ arcsec) has $(B - I)_{AB} = 1.39$, a colour similar to the bluest galaxies in this sample (1029, 1064 and the AGN 1843) and indicating an observer-frame visible flux dominated by young stars. This very interesting object is a red spiral with ongoing SF, apparently of long duration, concentrated in the outermost rim.

2246 ([O II] emitter) is a small, roundish, high-SB spheroid. In the B band it looks even more smaller, and asymmetric, suggesting a post-merger with central SF.

1823 ([O II] emitter) is a merger of nuclear separation $\simeq$0.3 arcsec, apparently of a spheroid (N) and a more irregular galaxy (S) with a lower I-band SB and three intensity peaks. In B the N spheroid is barely visible (passive?) but the S irregular is bright (starburst?).

1955 (no [O II]) is a high-SB spheroid with slight asymmetry in the outer regions, possibly due to perturbation by a smaller neighbouring galaxy separated by 0.8 arcsec separation. B morphology is similar but faint.

1762 ([O II] emitter) resembles several of the disc mergers in the Arp catalogue. The I image shows two nuclei separated by 0.34 arcsec, of which the larger (N) is at the centre of a partial ring or curved tail of radius $\simeq$0.4 arcsec, and the smaller (S) has a long ($\leqslant$1.0 arcsec) straight tail. In the B band the system appears much more fragmented, the large nucleus is less prominent but the S nucleus is bright and parts of the tails are visible, together with a bright region in the SW. This is a merger with extensive SF, and some of the bright clumps in the tails might be new dwarf galaxies being formed in the interaction.

1843 (> 1.5, *Chandra* source, AGN) has a central SB twice that of the other spheroidals in this sample. It appears to be a bright point source within a faint extended host galaxy visible in both I and B.

1158 ([O II] emitter) is of very low SB in the I band. It is more prominent on the K-band image. It appears to be an almost edge-on disc or ring some 1.6 arcsec in long-axis diameter, without a bright nucleus and without much asymmetry. In B it is even fainter and almost invisible, even with smoothing, but probably of similar size and shape. It is most likely a red spiral galaxy with the 'ring' appearance suggesting that most SF is in the outer regions rather than the nucleus (as in 1876?).

Sizes (half-light radii, r_{hl}) were estimated for the ERGs by fitting the profile of each in the *HST*-ACS Z_{850} band (approximately the rest-frame B band) with the Sersic profile $I(r) = I_0 = \exp[(r/r_0)^{1/n}]$, using a method in which this was convolved with the detailed form of the *HST*-ACS PSF (see Floyd et al. 2004). In this equation n is the Sersic index, $n = 1$ for an exponential (pure disc) profile and $n = 4$ for a de Vaucouleurs bulge profile. The half-light radius r_{hl} is a function of r_0 and n. Table 5 gives PSF-corrected r_{hl} and n for the 16 ERGs; note that two galaxies were not well represented by a single Sersic profile and have been fitted with two-component models.

Morphologically, these ERGs can be placed into three broad classes: (i) spheroidals of high Sersic index $\langle n \rangle = 4.39 \pm 0.40$

Table 2. Redshift z_{spec} (from emission lines, z_{em}, where detected, otherwise from continuum fits, z_{cf}); best-fitting age of the passively evolving component (T_{pas}); fraction f_{sb} of the flux at $\lambda_{rest\,frame} = 4500$ Å produced by the starburst component; age T_{sb} of the constant-SFR starburst; dust reddening $E(B-V)$ of the starburst (magnitudes); mean stellar formation redshift (z_{msf}) corresponding to the sum of T_{pas} and the look-back time of z_{spec}; and the best-fitting model mass for the passive (M_{pas}) and starburst (M_{sb}) stellar populations (normalized to the 2.0-arcsec aperture fluxes), in units of the solar mass $M_\odot$; Mf_{sb}, the starburst component as a fraction of the total stellar mass. Errors are approximately 90 per cent confidence intervals.

ID no.	z_{spec}	T_{pas} (Gyr)	f_{sb}	T_{sb} (Myr)	$E(B-V)$	z_{msf}	M_{pas}	M_{sb}	Mf_{sb}
1152	1.310	$1.5^{+0.1}_{-0.6}$	$0.035^{+0.01}_{-0.03}$	800^{+0}_{-780}	$0.0^{+0.1}_{-0}$	$1.95^{+0.06}_{-0.30}$	1.58×10^{11}	7.36×10^{8}	0.0046
1029	1.221	$1.0^{+0.5}_{-0.2}$	$0.105^{+0.03}_{-0.075}$	600^{+200}_{-560}	$0.0^{+0.05}_{-0}$	$1.68^{+0.25}_{-0.09}$	3.23×10^{10}	6.58×10^{8}	0.0199
1412	1.092	$1.0^{+0.2}_{-0.1}$	$0.06^{+0.045}_{-0.03}$	800^{+0}_{-200}	$0.5^{+0}_{-0.1}$	$1.39^{+0.08}_{-0.04}$	4.70×10^{10}	6.22×10^{9}	0.1168
1777	1.223	2.0 ± 0.2	$0.135^{+0.005}_{-0.045}$	800^{+0}_{-400}	$0.5^{+0}_{-0.05}$	$2.08^{+0.13}_{-0.12}$	1.08×10^{11}	1.70×10^{10}	0.1355
2536	1.512	0.6 ± 0.05	$0.04^{+0.03}_{-0.01}$	10^{+30}_{-0}	$0.5^{+0}_{-0.05}$	1.78 ± 0.03	6.17×10^{10}	8.20×10^{8}	0.0131
1064	1.548	1.0 ± 0.15	$0.09^{+0.005}_{-0.03}$	40^{+60}_{-30}	0.2 ± 0.1	$2.04^{+0.10}_{-0.09}$	1.47×10^{11}	1.31×10^{9}	0.0089
1143	1.254	$4.5^{+1.1}_{-2.1}$	$0.129^{+0.014}_{-0.042}$	10^{+10}_{-0}	$0.3^{+0.05}_{-0.1}$	$7.23^{+\infty}_{-4.79}$	7.29×10^{10}	1.89×10^{8}	0.0026
1565	1.108	$2.0^{+0.2}_{-0.6}$	$0.090^{+0.045}_{-0.015}$	10^{+200}_{-0}	$0.5^{+0}_{-0.05}$	$1.85^{+0.10}_{-0.28}$	3.87×10^{10}	3.38×10^{8}	0.0087
2401	1.200	$2.5^{+0.2}_{-0.1}$	$0.0^{+0.015}_{-0}$	–	–	$2.37^{+0.17}_{-0.07}$	1.63×10^{11}	0	0
1876	1.196	$1.5^{+0.3}_{-0.1}$	$0.05^{+0.04}_{-0.02}$	200^{+600}_{-140}	$0.5^{+0}_{-0.1}$	$1.75^{+0.16}_{-0.04}$	1.94×10^{11}	5.10×10^{9}	0.0256
2246	1.195	$2.0^{+0.5}_{-0.2}$	0.03 ± 0.024	800^{+0}_{-790}	$0.0^{+0.2}_{-0.0}$	$2.02^{+0.34}_{-0.11}$	8.27×10^{10}	2.64×10^{8}	0.0032
1823	0.868	$4.5^{+0.7}_{-1.7}$	$0.20^{+0.025}_{-0.05}$	800^{+0}_{-100}	$0.5^{+0}_{-0.05}$	$2.98^{+1.09}_{-1.25}$	1.91×10^{11}	2.36×10^{10}	0.1100
1955	1.180	$2.5^{+0.2}_{-0.3}$	$0.08^{+0.01}_{-0.05}$	800^{+0}_{-200}	$0.5^{+0}_{-0.1}$	$2.32^{+0.16}_{-0.21}$	1.43×10^{11}	1.07×10^{10}	0.0695
1762	1.102	$1.5^{+0.1}_{-0.5}$	$0.12^{+0.015}_{-0.005}$	10^{+5}_{-0}	0.4 ± 0.05	$1.60^{+0.04}_{-0.19}$	9.35×10^{10}	8.89×10^{8}	0.0094
1843[a]	2.017	$1.5^{+0.1}_{-0.7}$	$0.22^{+0.02}_{-0.04}$	10^{+5}_{-0}	0.4 ± 0.05	$3.42^{+0.16}_{-0.81}$	1.85×10^{11}	3.63×10^{9}	0.0193
1158	1.379	$3.5^{+0.6}_{-1.5}$	$0.075^{+0.045}_{-0.060}$	200^{+600}_{-180}	$0.5^{+0}_{-0.1}$	$4.59^{+2.53}_{-2.17}$	1.21×10^{11}	2.22×10^{9}	0.0183

Note: [a]Host galaxy of obscured AGN – age/mass estimates may be affected by non-stellar component.

Table 3. Nine-band (*HST*-ACS, ISAAC and Spitzer IRAC) photometry of the 16 ERGs in the redshift sample, with fluxes measured in fixed 2.0 arcsec diameter circular apertures (2.8 arcsec for Spitzer data) and expressed in the *AB* magnitude system, where $m_{AB} = -48.60$ to $2.5 \log F_\nu$ and 1 μJy is $m_{AB} = 23.90$. Absolute magnitude in rest-frame B (*AB* system), as estimated from the model fit to the aperture photometry (M_B), and with an approximate correction to total magnitude M_{BT}.

ID no.	$B_{435}(AB)$	$V_{606}(AB)$	$I_{775}(AB)$	$Z_{850}(AB)$	$J(AB)$	$H(AB)$	$K_s(AB)$	3.6 μm	4.5 μm	M_B	M_{BT}
1152	26.06	25.13	23.83	22.88	21.83	21.43	21.16	20.21	19.93	−21.51	−21.69
1029	25.85	25.56	24.58	23.62	22.79	22.32	22.11	21.27	21.00	−20.43	−20.49
1412	26.03	24.94	23.70	22.84	22.06	21.65	21.21	20.29	20.02	−20.77	−20.91
1777	n.d.	25.13	24.07	23.11	22.06	21.75	20.90	20.04	19.79	−20.95	−21.14
2536	25.71	25.04	24.07	23.47	22.48	22.10	21.51	20.79	20.52	−21.70	−21.77
1064	25.14	24.76	23.92	23.12	21.78	21.57	20.94	20.08	19.81	−22.06	−22.18
1143	27.28	25.47	25.40	24.78	23.33	22.76	22.15	21.37	21.10	−19.73	−19.81
1565	27.08	25.92	24.50	23.73	23.11	22.56	21.69	20.88	20.61	−19.79	−19.87
2401	27.42	25.71	24.18	22.97	21.97	21.23	20.95	20.43	20.16	−21.03	−21.21
1876	25.64	24.25	23.20	22.23	21.29	21.13	20.39	19.60	19.31	−21.75	−22.06
2246	26.81	25.81	24.39	23.41	22.38	22.22	21.54	20.90	20.63	−20.53	−20.55
1823	27.07	24.74	23.21	22.58	21.78	20.99	20.53	20.15	19.88	−20.86	−20.94
1955	27.35	25.69	24.01	22.81	21.70	21.52	20.89	20.06	19.78	−20.99	−21.13
1762	25.21	24.23	23.29	22.43	21.87	21.34	20.74	20.12	19.86	−21.06	−21.06
1843	25.62	25.16	24.55	24.15	23.05	22.36	22.02	21.27	21.00	−21.96	−22.14
1158	n.d.	26.99	25.09	24.16	23.46	22.54	21.85	20.65	20.38	−20.35	−20.58

Note: n.d. = not detected (too faint) in this passband.

(1152, 1029, 1143, 2401, 2246, 1955, 1843), (ii) red disc or spiral galaxies, of low Sersic index (exponential profiles) $\langle n \rangle = 1.05 \pm 0.05$ and without much sign of disturbance (1412, 1777, 1876, 1158) and (iii) merging or highly disturbed galaxies (2536, 1064, 1565, 1823, 1762) typically with intermediate Sersic indices $\langle n \rangle = 1.78 \pm 0.43$.

Fig. 6 shows the Sersic model r_{hl} for the 16 ERGs plotted against the estimated total absolute magnitude (the M_{BT} from Table 3).

Also plotted for comparison are, firstly, a mean $r_{hl} - M_B$ relation for local galaxies, as derived from the Driver et al. (2005) relation of B-band effective surface brightness to absolute magnitude for the Millenium Galaxy Catalogue, converted to $H_0 = 70$ and *AB* magnitudes ($B_{AB} = B_{MGC} - 0.13$). This sample is composed predominantly of spirals. Secondly, to represent local spheroidals we plot the best-fitting size–luminosity relation of early-type (Sersic $n > 2.5$) galaxies in the Sloan Digital Sky Survey (SDSS;

Table 4. Equivalent width of the [O II] 3727 Å emission line, converted to rest frame, the line flux ($f_{O\,II}$) and luminosity ($L_{O\,II}$), and the SFR derived from this (SFR $_{O\,II} = 1.4 \times 10^{-41} L_{O\,II}$ M$_\odot$ yr^{-1}), for ERGs in our redshift sample (these quantities normalized to the ERG flux in a 2.0 arcsec diameter aperture). 1σ upper limits are given for galaxies where no [O II] emission is seen.

ID no.	EW [O II] Å rest frame	$f_{O\,II}$ 10^{-18} erg s^{-1} cm^{-2}	$L_{O\,II}$ 10^{40} erg s^{-1}	SFR$_{O\,II}$ M$_\odot$ yr^{-1}
1152	5	8.40 ± 2.90	9.21 ± 3.18	1.29 ± 0.45
1029	46	38.1 ± 2.8	35.1 ± 2.5	4.91 ± 0.35
1412	9	11.34 ± 2.45	7.88 ± 1.70	1.10 ± 0.22
1777		< 3.33	< 3.08	< 0.43
2536	?	?	?	?
1064	?	?	?	?
1143	21	7.38 ± 2.13	7.21 ± 2.08	1.01 ± 0.29
1565	31	15.85 ± 2.34	11.43 ± 1.69	1.60 ± 0.24
2401	< 2.41	< 2.12	< 0.30	
1876	5	10.26 ± 2.76	8.94 ± 2.35	1.25 ± 0.33
2246	12	10.22 ± 1.57	8.91 ± 1.37	1.25 ± 0.19
1823	10	18.58 ± 1.65	7.26 ± 0.65	1.02 ± 0.08
1955		< 2.20	< 1.86	< 0.26
1762	8	10.48 ± 3.32	7.45 ± 2.35	1.04 ± 0.33
1843	?	?	?	?
1158	40	10.51 ± 3.36	13.13 ± 4.20	1.84 ± 0.59

?: galaxy is at $z > 1.5$ where [O II] 3727 Å would not be visible in GMOS λ range.

Shen et al. 2003), with an approximate conversion $B_{AB} = r + 1.17$ (Driver et al. 2005).

Amongst spheroidal and disc ERGs, there is considerable scatter in the size–luminosity relation, but generally little, or moderate (<1 mag) enhancement in SB relative to local galaxies of the same type. This would be consistent with the passive evolution of ellipticals which formed Gyr earlier, or with the exponentially declining SFRs of early-type spirals. One ERG, the disc 1158, has a significantly lower SB than a typical local galaxy and on the basis of its spectrum (Fig. 3) this is likely due to heavy internal dust extinction, as well as a diffuse morphology. Merging ERGs, in contrast, show in their size–luminosity relation a marked (1–2 mag) SB brightening relative to local galaxies, especially in the case of the $z > 1.5$ mergers 2536 and 1064, presumably due to intense, short-term starbursts.

6 ERG CLUSTERING VERSUS PHOTOMETRIC REDSHIFT

We re-examine the clustering of ERGs in the CDFS sample using the photometric redshift estimates of Caputi et al. (2004, 2005), which will allow us to obtain a more reliable and less model-dependent estimate of their clustering properties than given in RDA03.

The angular correlation function, $\omega(\theta)$, is a measure of the clustering of galaxies as projected on the plane of the sky. It is related to the *intrinsic* clustering in three dimensions, parametrized by the correlation radius r_0, by means of an integration known as Limber's formula (see e.g. Efstathiou et al. 1991; RDA03)

If the two-point correlation function, expressed in proper coordinates, $\xi(r)$ is represented by the simple model

$$\xi(r, z) = \left(\frac{r}{r_0} \right)^{-\gamma} (1 + z)^{-(3+\epsilon)},$$

where $\gamma \simeq 1.8$ (observationally) and ϵ represents the clustering evolution ($\epsilon = 0$ is stable and $\epsilon = -1.2$ is comoving clustering). Then Limber's formula gives $\omega(\theta) = A_\omega \, \theta^{-(\gamma-1)}$, where

$$A_\omega = C_\gamma r_0^\gamma \int_0^\infty \frac{(1+z)^{\gamma-(3+\epsilon)}}{x^{\gamma-1}(z)\,[\mathrm{d}x(z)/\mathrm{d}z]}$$
$$\times \left[(N(z)^2 \right]\, \mathrm{d}z \Bigg/ \left[\int_0^\infty N(z)\,\mathrm{d}z \right]^2,$$

where $x(z)$ is the proper distance and $C_\gamma = 3.679$ for $\gamma = 1.8$.

Hence, in order to estimate r_0 from the observable A_ω, a model or observed $N(z)$ is required, and for deep samples, the r_0 will also depend on ϵ. However, we can also express the clustering measured at any redshift in terms of a comoving correlation radius r_{c0}, without any assumptions about ϵ, as in comoving space

$$\xi(r_c, z) = \left(\frac{r_c}{r_{c0}} \right)^{-\gamma}.$$

In this system, comoving clustering would be a constant r_{c0} and stable clustering would be $r_{c0} \propto (1 + z)^{-2/3}$.

Previously (RDA03) we calculated the angular correlation function, $\omega(\theta)$ of the CDFS ERGs. We obtained a $\sim 3\sigma$ detection of clustering at the completeness limit of $K_s \leqslant 21.5$, which appeared consistent with the ERG $\omega(\theta)$ measurements of Daddi et al. (2000), Firth et al. (2002) and Roche et al. (2002). By combining all these we estimated $r_{c0} = 12.5 \pm 1.4 \, h^{-1}$ Mpc for ERGs. However, this estimate is dependent on a model $N(z)$, taken from a 'merging and negative density evolution' model, fitted to the ERG number counts without any redshift data. Furthermore, the clustering evolution remains undetermined.

We can now obtain a less model-dependent estimate of r_{c0}, and investigate ϵ, by including redshift data. We assign to each ERG a redshift estimate, which for the 16 galaxies in our redshift sample is the GMOS spectroscopic redshift and for the remainder, the photometric redshift estimate from Caputi et al. (2004, 2005). Objects with $z_{phot} > 4$ are assigned redshifts following section 4.6 of Caputi et al. (2004), in which only two ERGs with $K_s < 22$ (one with $K_s < 21.5$) are accepted as probable $z > 4$ galaxies, and four of our original sample are reclassified as stars.

Fig. 7 shows the distribution of true/estimated redshifts for the 175 ERGs brighter than the approximate completeness limit $K_s = 21.5$. The photometric $N(z)$ is quite close to the RDA03 model, especially at the peak, although more dispersed to lower and higher redshifts, presumably as real galaxies are more varied in their evolution.

The angular correlation functions $\omega(\theta)$ were calculated for the CDFS ERGs using the same methods as in RDA03. Each $\omega(\theta)$ was fitted with the function '$A_\omega(\theta^{-0.8} - 12.24)$' (see RDA03), to obtain a power-law amplitude, A_ω. The errors on the A_ω were estimated using the same 'bootstrap' method as RDA03 (essentially repeating the analysis for a series of data catalogues with small regions excluded and finding the scatter in the resulting estimates).

We first consider the full $K_s < 21.5$ sample of 175 ERGs. From its $\omega(\theta)$ amplitude measurement (Table 6) and photometric/spectroscopic $N(z)$ (Fig. 7), Limber's formula gives the comoving correlation radius $r_{c0} = 13.13^{+2.12}_{-2.44} \, h^{-1}$ Mpc. This is consistent with the RDA03 estimate based on a model $N(z)$. Alternatively, if we set $\epsilon = 0$ this result can be fit with a stable clustering model with $r_0 = 23.91^{+3.86}_{-4.44} \, h^{-1}$ Mpc (at $z = 0$).

We then recalculate $\omega(\theta)$ for the ERGs divided into two subsamples in phot/spec redshift. For both the low- and high-redshift subsamples, the $\omega(\theta)$ and $N(z)$ are used to derive a comoving r_{c0} (Table 6). Dividing the sample reduces the significance of
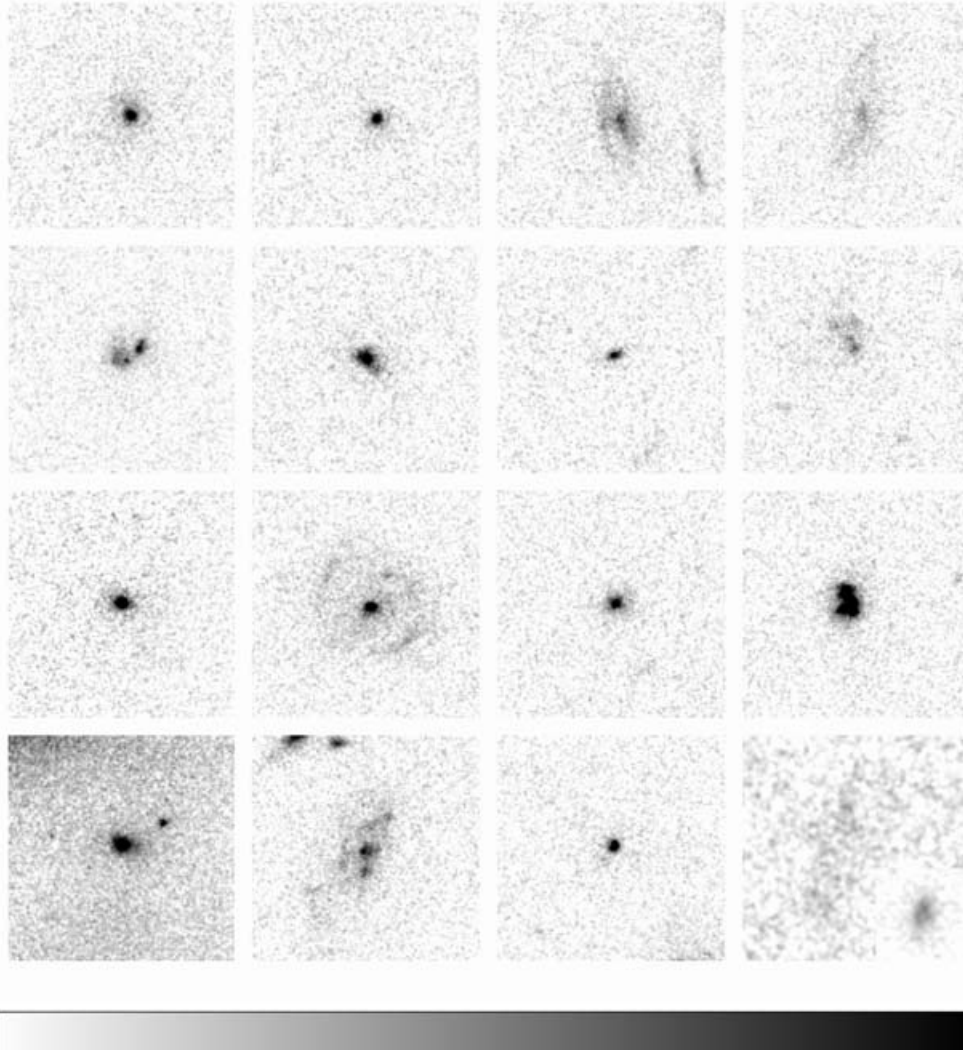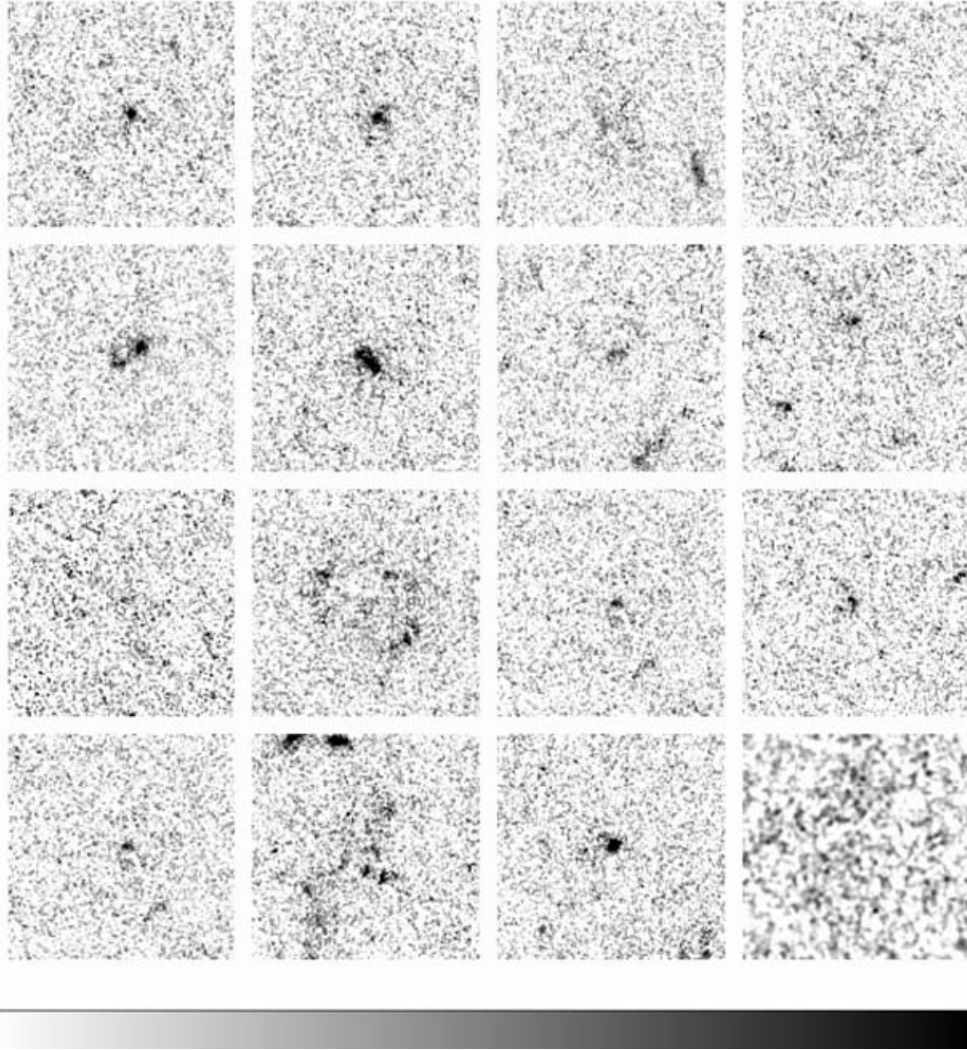
Figure 4. ACS I_{775}-band images, from the GOODS data version v1.0, of the 16 ERGs in our redshift sample: (top row, left- to right-hand side) 1152, 1029, 1412, 1777; (second row) 2536, 1064, 1143, 1565; (third row) 2401, 1876, 2246, 1823; (bottom row) 1955, 1762, 1843, 1158. Each picture shows a 3.9×3.9-arcsec^2 area, with an inverse grey-scale with black corresponding to $22.27\,AB$ mag arcsec^{-2}. Galaxy 1158, due to its very low SB, is shown smoothed by a FWHM = 0.07 arcsec Gaussian and scaled up in intensity by a factor of 2, and its ISAAC K_s-band image is shown inset in the lower right-hand side (at a scale 0.4 that of its ACS image).

clustering detection, but in most cases it remained $>2\sigma$. We repeat this analysis for redshift divides at $z = 1.4$, 1.6 and 1.8.

The subset $\omega(\theta)$ amplitudes are given in Table 6 and plotted in Fig. 8. It can immediately be seen that the mean of the r_{c0} we derive for the low- and high-redshift subsamples is a little lower than that of the full K-limited sample, by about 19 per cent, which corresponds to 32 per cent in the A_ω. The reason for this is that photometric redshifts are not always accurate and thus the low- and high-redshift subsamples will both experience some contamination from galaxies in the other redshift range, which are not correlated with the correctly selected galaxies and dilute the observable clustering. If, for example, the true $\omega(\theta)$ of the lower redshift ERGs is A_l and of the high A_h, and we examine a low z_{phot} subsample with a contamination α, the $\omega(\theta)$ we calculate will be $A_{obs} \simeq (1 - \alpha)^2\, A_l + \alpha^2\, A_h$. The observed shortfall could be accounted for by $\alpha \simeq 0.20$. We have not attempted to correct for this is deriving a r_{c0}, and thus the low- and high-redshift r_{c0} will both be slight underestimates (by similar amounts, as here the two subsamples have similar size and clustering).

Secondly, the higher redshift subsamples have a comoving r_0 similar to or even a little greater than the lower redshift ERGs. This is clearly more consistent with comoving clustering rather than stable clustering. The slight increase in r_{c0} with redshift, if real could reflect a stronger clustering for more massive/luminous ERGs. Comoving clustering of $r_0 \simeq 12$–$13\,h^{-1}$ Mpc is consistent with the clustering of both shallower (Daddi et al. 2000) and deeper ERG samples, e.g. Daddi et al. (2004) estimate $r_0 = 9$–$17\,h^{-1}$ Mpc at $1.7 < z < 2.3$. Extrapolated to lower redshifts, this model would overpredict the clustering of local passive galaxies of all luminosities, $r_0 = 7.2\,h^{-1}$ Mpc (Madgwick et al. 2003), but be consistent with the clustering of the most luminous ($M_R < -22.27$) early-types at $0.3 < z < 0.9, r_0 = 11.2 \pm 1.0\,h^{-1}$ Mpc comoving (Brown et al. 2003). This can be explained if (i) many of the $z > 1$ ERGs undergo further merging to become very massive ellipticals, (ii) only some ($\sim$ half) of the moderate-luminosity E/S0s found locally have evolved directly from $z > 1$ ERGs and the others are formed at $z \leqslant 1$ from mergers of less strongly clustered spirals, thus diluting the clustering.

Figure 5. ACS B_{450}-band images, from the GOODS data version v1.0, of the 16 ERGs in our redshift sample: (top row, left- to right-hand side) 1152, 1029, 1412, 1777; (second row) 2536, 1064, 1143, 1565; (third row) 2401, 1876, 2246, 1823; (bottom row) 1955, 1762, 1843, 1158. Each picture shows a 3.9 × 3.9-arcsec^2 area, with an inverse grey-scale with black corresponding to 24.03 *AB* mag arcsec^{-2}. Galaxy 1158, due to its very low SB, is shown smoothed by a FWHM = 0.07 arcsec Gaussian and scaled up in intensity by a factor of 2.

To better understand the evolution of ERGs it will be useful to compare their clustering with that of their likely progenitors at higher redshifts, such as sub-mm galaxies, for which the clustering will be measured in the ongoing SHADES survey. There is already evidence that the most massive Lyman break galaxies at $z \sim 4$ have a similar comoving $r_0(11.4 \pm 2\,h^{-1}\,\text{Mpc})$ to the $z \sim 1$–2 ERGs (Allen et al. 2005).

7 DISCUSSION

7.1 Ages of ERGs

We perform spectroscopic age-dating of the ERGs by fitting their SEDs with passively evolving models (from Jimenez et al. 2004), and obtain mean stellar ages ranging widely from 0.6 to 4.5 Gyr, with a mean of 2.1 ± 0.3 Gyr. We can compare these results with similar age-dating analyses performed by other authors, though must be careful to consider the differences in how the sample are selected. First, Daddi et al. (2004) give ages (from FORS2 spectra) for nine K-selected ($K_s < 20$) very massive star form-

ing galaxies at $1.7 < z < 2.3$ – note that not all of these are red enough to be called ERGs. Daddi et al. (2005) give ages from low-resolution ACS spectra of seven ERGs at $1.39 < z < 2.47$, of which five are passive ellipticals and two weakly star forming. McCarthy et al. (2004) using Gemini Deep Survey spectra, give ages for a varied sample of 20 red ($I - K > 3.5$) galaxies at $1.3 < z < 2.2$. Finally, Longhetti et al. (2005) using low-resolution NIR spectra (observed with NICS on the La Palma TNG), estimate mass-weighted ages for 10 of the most bright ($K' = 16.6$–18.4) and massive (10^{11}–$10^{12}\,\text{M}_\odot$) ERGs ($R - K' > 5.0$) present at $z \sim 1.5$.
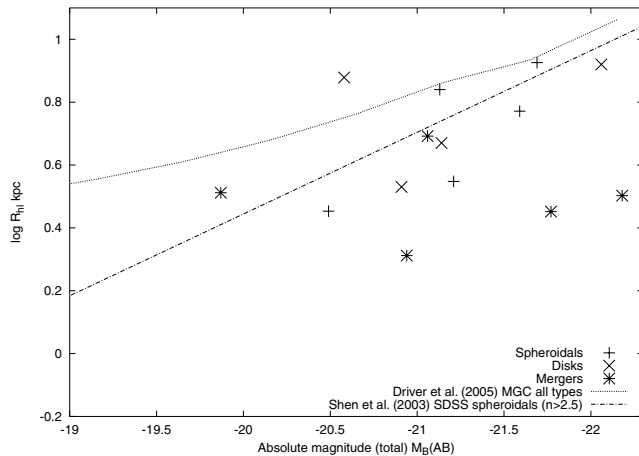
Fig. 9 plots stellar age T_{pas} against spectroscopic redshift for all these samples, with loci of the redshifts corresponding to time T_{pas} before observation.

For the first four samples the mean stellar ages of ERGs at all $1 < z < 2.5$ are spread over the range between $z \sim 5$ and shortly (a few times 10^8 yr) before the epoch of observation. They seem to divide into two groups with $z_{\text{msf}} \sim 2$ and $z_{\text{msf}} \sim 3$–4.

The Longhetti et al. (2005) sample of very luminous ERGs differs from the others in that it seems to be concentrated towards higher

Table 5. Half-light radius and Sersic index of the ERGs from model profiles fitted to *HST*-ACS Z_{850}-band images. Galaxy 1876 is fitted as a combination disc ($n = 1$) plus bulge ($n = 4$), and galaxy/AGN 1843 as a combination bulge plus point source ($n = 0$).
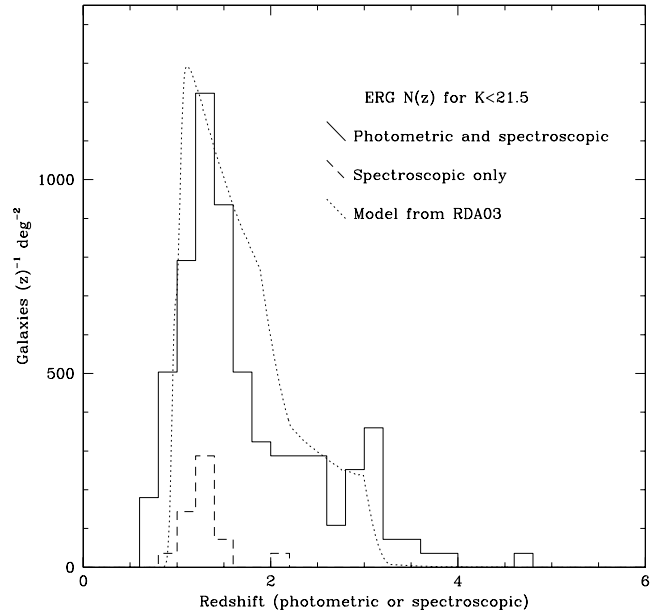
ID no.	Sersic index n	$r_{\rm hl}$ (arcsec)	$r_{\rm hl}$ (kpc)
1152	4.8	0.969	8.43
1029	5.1	0.330	2.84
1412	1.2	0.402	3.39
1777	1.0	0.543	4.68
2536	1.4	0.321	2.83
1064	3.5	0.360	3.18
1143	2.4	0.054	0.47
1565	1.4	0.384	3.25
2401	5.8	0.411	3.53
1876	(85 per cent) 1.0	0.969	8.32
	(15 per cent) 4.0	0.060	0.52
2246	4.2	0.261	2.24
1823	1.2	0.258	2.05
1955	4.4	0.807	6.92
1762	1.4	0.582	4.92
1843	(60 per cent) 4.0	0.675	5.91
	(40 per cent) 0.0	–	–
1158	1.0	0.864	7.56

Figure 7. The distribution $N(z)$ of photometrically estimated (Caputi et al. 2004, 2005), or spectroscopic (this paper) redshifts for the 175 $K_s \leqslant 21.5$ ERGs in our CDFS sample (solid histogram); spectroscopic redshifts only (dashed histogram) and the best-fitting model ERG $N(z)$ from RDA03 (dotted line).

Table 6. Angular correlation function [$\omega(\theta)$] amplitudes (given at $\theta = 1°$ for a fitted $\theta^{-0.8}$ power law), estimated for CDFS ERGs, to a limit $K_s = 21.5$ (Vega system), divided into two subsamples in photometric/spectroscopic redshift. This is shown for redshift divides $z = 1.4$, 1.6 and 1.8.

$z_{\rm phot/spec}$ range	$z_{\rm mean}$	Number of ERGs	$\omega(\theta)$ amplitude 10^{-3} (deg $^{0.8}$)	r_{c0} (h^{-1} Mpc)
All	1.742	175	6.54 ± 2.02	$13.31^{+2.12}_{-2.44}$
$z < 1.4$	1.125	72	10.94 ± 3.89	$9.63^{+1.78}_{-2.08}$
$z > 1.4$	2.187	103	7.39 ± 4.22	$11.39^{+3.25}_{-4.27}$
$z < 1.6$	1.231	101	6.61 ± 2.93	$8.45^{+1.91}_{-2.35}$
$z > 1.6$	2.458	74	8.34 ± 3.46	$12.32^{+2.62}_{-3.17}$
$z < 1.8$	1.273	111	6.42 ± 2.89	$9.03^{+2.03}_{-2.56}$
$z > 1.8$	2.577	64	12.41 ± 4.70	$14.04^{+2.74}_{-3.26}$

Figure 6. Half-light radius from fitted Sersic model plotted against total absolute magnitude in B_{AB}, for the 16 ERGs in the redshift sample (symbols indicate morphology). For the AGN 1843 only the 60 per cent extended component of the flux is included in the plotted absolute magnitude (giving $M_B = -21.59$). Also plotted are the mean size–luminosity relations for galaxies in the Millenium Galaxy Catalogue, derived from Driver et al. (2005), and for early-type galaxies in the SDSS (Shen et al. 2003).

formation redshifts – it contains five galaxies with $z_{\rm msf} > 5$. These have stellar masses 3.8–9.4×10^{11} M$_\odot$, more than twice the mass of any ERG in our sample. Hence, their ages may be evidence that the very most massive spheroidals formed significantly earlier and/or formed their stars most quickly, as in the model of Granato et al. (2004).

It is also notable that the formation redshifts appear to trace the plotted $z_{\rm msf}$ loci. The ages of the oldest galaxies at each redshift, as a function of redshift, is an important tracer of the expansion of the Universe and hence the cosmological model (e.g. Jimenez & Loeb 2002). We would expect $z_{\rm msf}$ for the oldest galaxies to be constant with observed redshift, and the agreement with the plotted

loci would support a $\Lambda \simeq 0.75$ cosmological constant ($w = -1$) model.

As $T_{\rm pas}$ represents a flux-weighted mean stellar age, the true age of a galaxy since formation must always be greater, to a degree dependent on the detailed form of the SF history. One interpretation may therefore be that most or all of the red galaxies observed as ERGs at $z = 1$–2 are galaxies, or mergers of galaxies, which formed at $z \geqslant 4$–5, and that the spread in their stellar ages up to this maximum redshift can be attributed to differences in their individual evolution, i.e. the mergers and starbursts they have experienced.

Caputi et al. (2004, 2005), using photometric redshift estimates derived from seven-band photometry of ERGs and other $K < 22$ galaxies in this field, found the comoving number density of massive ($> 5 \times 10^{10}$ M$_\odot$) galaxies in a full K-selected sample to fall only slowly from $z = 1.75$ to 3.5, where a significant fraction, 20–25 per cent, of today's massive galaxies were already in place. However, the comoving number density of the reddest subset of these galaxies, the ERGs, evolves much more rapidly, steadily increasing with time
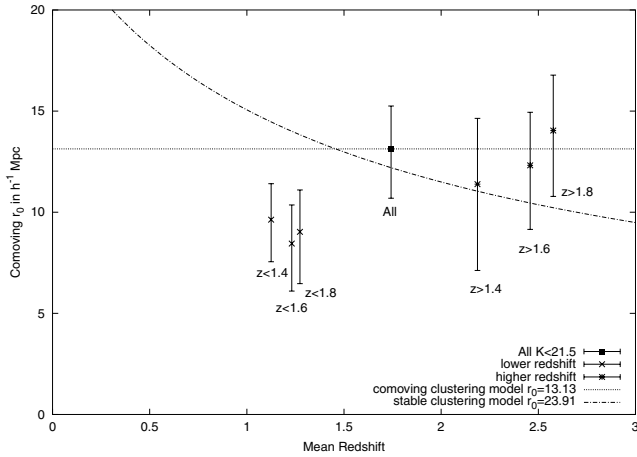
Figure 8. Comoving correlation radius r_{c0}, derived from the $\omega(\theta)$ amplitude and photometric $N(z)$, for a full $K_s < 21.5$ sample of ERGs, and for these ERGs divided by photo-z into low- and high-redshift subsamples (dividing at $z = 1.4$, 1.6 and 1.8) plotted against sample mean redshift. Also plotted are comoving ($\epsilon = -2$) and stable-clustering ($\epsilon = 0$) models normalized to the full sample's clustering.
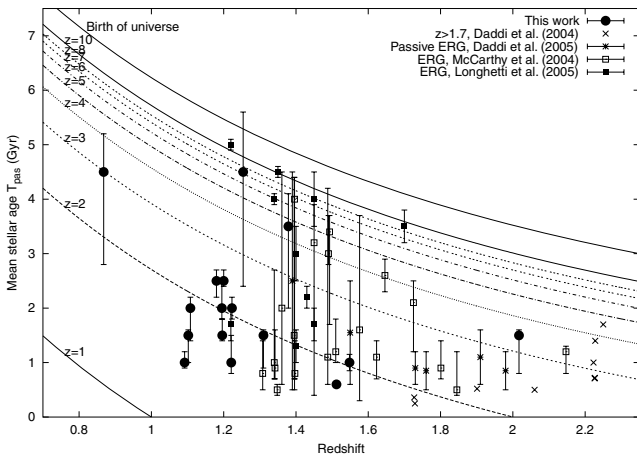
Figure 9. Mean stellar age T_{pas}, derived from model fitting to spectra, against redshift for our ERG sample, the K-selected galaxies of Daddi et al. (2004), and the ERGs of Daddi et al. (2005), McCarthy et al. (2004) and Longhetti et al. (2005). Plotted loci show the redshifts corresponding to time T_{pas} before the redshift of observation.

from $z = 3.5$ to 1, and following a trend which extrapolates to the present-day E/S0 population at $z = 0$. At $z = 1$–1.5, the rising comoving number density of ERGs approached that of all K-selected galaxies at the higher redshift of $z \sim 3.5$.

Hence, this suggests that a substantial population of massive galaxies formed at $z \geqslant 4$ and were initially starbursting and relatively blue, but with increasing age many became red enough to be classed as ERGs. Interestingly, for the brightest ($I < 24.5$) Lyman break galaxies at $z \sim 4$, Allen et al. (2005) measure strong clustering of $r_0 = 11.4 \pm 2\,h_{100}^{-1}$ Mpc comoving, consistent with these evolving into the ERGs at $z = 1$–2.

To produce the evolution in ERG number density these galaxies must have entered the ERG class over a wide redshift range $1 < z < 4$, again implying much variation in their SF histories. The formation of so many massive galaxies at $z \geqslant 4$ places significant constraints on models of galaxy formation (e.g. Fontana et al. 2004)

and may favour models with feedback between the SF in formative spheroidals and the growth of supermassive black holes within them (Granato et al. 2004; Silva et al. 2005).

7.2 Ongoing SF activity in ERGs

Yan et al. (2004a) and Doherty et al. (2005) found that $\geqslant 75$ per cent of ERG spectra have prominent absorption features and 4000-Å breaks, while >50 per cent also show some [O II] emission. We find the same for our slightly deeper sample. For only three ERGs do we find neither [O II] emission nor any indication of a young stellar population from a blue excess in the SED. This is consistent with the Doherty et al. (2005) estimate that 28 per cent of ERGs show no evidence of recent SF.

For a clear majority of ERGs, 10/13 at $z < 1.5$, we detect a [O II] 3727 Å emission line. This includes two galaxies where the line only just detected with an equivalent width (EW) ~ 5 Å, while at the other extreme we have three ERGs with [O II] EWs $\geqslant 30$ Å. For the 10 emission-line galaxies, the [O II] 3727 Å fluxes – uncorrected for dust – correspond to a mean SFR of 1.63 $M_\odot$ yr^{-1}, intermediate between the 2.8 $M_\odot$ yr^{-1} mean SFR$_{O II}$ of Yan et al. (2004a) and the 1.1 $M_\odot$ yr^{-1} of the Doherty et al. (2005) ERGs.

Of course the true SFRs of the emission-line ERGs will be higher. On the basis of the dust extinction estimated from our model fits, we estimate the real mean SFR will be about 12–24 $M_\odot$ yr^{-1}. This may still be an underestimate as emission-line regions of current SF may suffer more extinction than the continuum produced by SF over a longer period. Spitzer mid-IR (Yan et al. 2004b) observations of ERGs similarly selected to those in our sample indicate that about half have SFR $> 12\,M_\odot$ yr^{-1}, and for these the mean SFR $\simeq 60\,M_\odot$ yr^{-1}. We should be able to obtain genuinely dust-independent measurements of the SFRs for the individual ERGs in the GOODS-S from the deep Spitzer 24-μm survey of this field scheduled for later this year.

7.3 Morphology and SF history

Examining the *HST*-ACS images of ERGs we find ERGs to be a mixture of spheroidals, spirals and merging systems. The classifications by eye are confirmed by Sersic model fits to the radial profiles (Table 4). We discuss the nature and SF activity of the ERGs within each of these morphological categories.

7.3.1 Spheroidals

We class seven ERGs, almost half the sample, as spheroidals. Spectroscopically they are varied, and this may be related to whether or not they have recently undergone a merger event or the accretion of a gas-rich galaxy. One spheroidal (2401) appears to be old and purely passive, with no evidence of SF in the last 2.5 Gyr. Another (1955) shows no [O II] emission but its NIR colours suggest it may be a dust-reddened post-starburst galaxy. One of the spheroidal ERGs hosts an obscured AGN, it may also be star forming. One is old with a young, dusty starburst (1143). The final three (2246, 1152, 1029) are relatively young (1–2 Gyr) with the model fits suggesting prolonged, low-level, non-dusty SF; and appear to show post-merging features.

7.3.2 Mergers

Of these 16 ERGs five are obvious mergers, with multiple nuclei, and all of these are star forming galaxies, on the basis of [O II]

emission. The two $z > 1.5$ mergers also have a high surface brightness (Fig. 6). Presumably, the SFRs and dust content are both increased by the interactions. Some appear to be mixed mergers of passive spheroidals with bluer irregulars (e.g. 1565 and 1823), and one (1762) has prominent tidal tails. On the basis of our model fits, four of the five mergers are relatively young (0.6–2.0 Gyr) and undergoing short-term (10–40 Myr) dusty starbursts. Notably, in our sample; four of the five galaxies with $T_{sb} < 50$ Myr are mergers (the other is an AGN). This would be expected from the current interaction acting to tidally trigger an intense but short-term starburst. The fifth merger, a close irregular/spheroidal pair, (1823) differs in that it is ∼4.5-Gyr old with a long T_{sb} and Balmer absorption. This may be explained if it is a late-stage merger where most starbursting occurred at earlier encounters of the two galaxies, and the elliptical is already very old.

7.3.3 Spirals

Perhaps a more surprising discovery is that of a third morphological class of ERGs which are neither ellipticals nor mergers, but red spirals. We find four of these. According to our model, the four spirals differ widely in age (1.0–3.5 Gyr) but in all cases contain a young component with a long T_{sb} (200–800 Myr) and heavy dust extinction [$E(B − V) \simeq 0.5$]. Three show [O II] emission, the fourth (1777) may therefore have ceased forming stars. Strong Balmer lines are seen in two of the spirals, 1412 and 1876, and this reinforces the evidence from model fits that spiral ERGs tend to contain large intermediate-age (0.1–1.0 Gyr) populations.

It is also notable that spiral 1876 has a luminous red (passive?) nucleus ringed by blue star forming regions, producing a strong colour gradient. Indeed, for three of the spiral ERGs, a comparison of the I and B images shows that (in contrast to the merging ERGs), their SF is not predominantly nuclear but in the outer discs. The $z = 1.55$ ERG #4950 of Daddi et al. (2005), classed as type Sa, also has a red nucleus with a blue outer ring.

The existence and spectral properties of very red spirals can be explained if they are galaxies with continuous SF which has been gradually slowed or completely truncated. This explains the long T_{sb}, Balmer absorption, and the absence of emission lines in one spiral (already truncated?). In addition to this, they are very dusty, as the ERG colour criterion would select out the spirals at the very top end of the wide range of internal dust extinctions.

Very red spiral galaxies also occur at lower redshifts, where they make up some 0.3 per cent of all galaxies (Yamauchi & Gotu 2004), and tend to be found in the outer regions of clusters (Couch et al. 2002; Goto et al. 2003). In the model of Bekki, Couch & Shioya (2002) a spiral galaxy, falling into a cluster, experiences a truncation of SF activity, as its gas content is removed through ram-pressure stripping by the intracluster medium and/or by cluster tidal fields. Following this the galaxy would become very red in ∼1 Gyr but could retain a spiral appearance, with visible arms, for $\geqslant 3$ Gyr, although would ultimately evolve into an S0 type. This mechanism could give rise to red spirals at ERG redshifts, as both spiral galaxies (Dawson et al. 2003) and large ERG-rich clusters (e.g. Kurk et al. 2004) are already in place at $z \geqslant 2$. However, some spiral ERGs, e.g. 1876, must be in relatively early stages of this process as much SF is still ongoing in their outer regions.

More information on the nature of spiral ERGs and the relative importance of dust and 'truncation' will soon be available from Spitzer 24-μm data, giving a dust-independent SFR, and spectroscopy at 1–2 μm, showing Balmer lines and Hα. It is likely that some sort of environmental effect is involved because ERGs in general are very much more clustered than typical spirals.

7.4 Further investigations

Ongoing surveys of the CDFS with the Spitzer Infrared Telescope will, when complete, provide accurate, dust-independent measurements of the SFRs in our redshift sample. The ongoing SHADES survey of bright, $F(850\,\mu m) > 8$ mJy, sub-mm galaxies will provide a measurement of the clustering of these probable progenitors of the ERGs (Dunlop 2005; Mortier et al. 2005). We have planned further and more extensive spectroscopic surveys, including in the NIR, of high-redshift galaxy clusters and large-scale structure.

REFERENCES

Abraham R. G. et al., 2004, AJ, 127, 2445
Alexander D. M., Vignali C., Bauer F. E., Brandt W. N., Hornschemeier E., Garmire G. P., Schneider D. P., 2002, AJ, 123, 1149
Allen P. D., Moustakas L. A., Dalton G., MacDonald E., Blake C., Clewley L., Heymans C., Wegner G., 2005, MNRAS, 360, 1244
Bekki K., Couch W., Shioya Y., 2002, ApJ, 577, 651
Brown M. J. I., Dey A., Jannuzi B. T., Lauer T. R., Tiede G. P., Mikles V. J., 2003, ApJ, 597, 225
Bruzual G., Charlot S., 2003, MNRAS, 344, 1000
Calzetti D., Armus L., Bohlin R. C., Kinney A. L., Koornneef J., Storchi-Bergmann T., 2000, ApJ, 533, 682
Caputi K. I., Dunlop J. S., McLure R. J., Roche N. D., 2004, MNRAS, 353, 30
Caputi K. I., Dunlop J. S., McLure R. J., Roche N. D., 2005, MNRAS, 361, 607
Cimatti A. et al., 2002, A&A, 381, 68
Cimatti A. et al., 2003, A&A, 412, L1
Couch W. J., Balogh M. L., Bower R. G., Smail I., Glazebrook K., Taylor M., 2001, ApJ, 549, 820
Daddi E., Cimatti A., Pozzetti L., Hoekstra H., Röttgering H., Renzini A., Zamorani G., Mannucci F., 2000, A&A, 361, 535
Daddi E. et al., 2004, ApJ, 600, L127
Daddi E. et al., 2005, ApJ, 626, 680
Dawson S., McCrady N., Stern D., Eckart M. E., Spinrad H., Liu M. C., Graham J. R., 2003, AJ, 125, 1236
de Mello D., Daddi E., Renzini A., Cimatti A., di Serego Alighieri A., Pozzetti L., Zamorani G., 2004, ApJ, 608, L29
Doherty M., Bunker A. J., Ellis R. S., McCarthy P. J., 2005, MNRAS, 361, 525
Driver S. P., Liske J., Cross N. J. G., De Propris R., Allen P. D., 2005, MNRAS, 360, 81
Dunlop J. S., Peacock J., Spinrad H., Dey A., Jimenez R., Stern D., Windhorst R., 1996, Nat, 381, 581
Dunlop J. S., 2005, Astrophys. Space Sci. Library Vol. 329, Starbursts: From 30 Doradus to Lyman Break Galaxies. Springer-Verlag, Dordrecht, p. 121

Efstathiou G., Bernstein G., Katz N., Tyson J. A., Guhathakurta P., 1991, ApJ, 380, L47

Firth A. E. et al., 2002, MNRAS, 332, 617

Floyd D. J. E., Kukula M. J., Dunlop J. S., McLure R. J., Miller L., Percival W. J., Baum S. A., O'Dea C. P., 2004, MNRAS, 355, 196

Fontana A. et al., 2004, A&A, 424, 23

Giacconi R. et al., 2002, ApJS, 139, 369

Giavalisco et al., 2004, ApJ, 600, L93

Goto T. et al., 2003, PASJ, 55, 757

Granato G. L., De Zotti G., Silva L., Bressan A., Danese L., 2004, ApJ, 600, 580

Hamuy M., Suntzeff N., Heathcote S., Walker A., Gigoux P., Phillips M., 1994, PASP, 106, 700, 566

Jimenez R., Loeb A., 2002, ApJ, 573, 37

Jimenez R., MacDonald J., Dunlop J. S., Padoan P., Peacock J. A., 2004, MNRAS, 349, 240

Kennicutt R., 1998, ARA&A, 36, 189

Kurk J. D., Pentericci L., Röttgering H. J. A., Miley G. K., 2004, A&A, 428, 793

Longhetti M. et al., 2005, MNRAS, 361, 897

Madgwick D. S. et al., 2003, MNRAS, 344, 847

McCarthy P. J. et al., 2004, ApJ, 614, L9

Mortier A. M. J. et al., 2005, MNRAS, 363, 509

Roche N. D., Almaini O., Dunlop J. S., Ivison R. J., Willott C. J., 2002, MNRAS 337, 1282

Roche N. D., Dunlop J. S., Almaini O., 2003, MNRAS, 346, 803 (RDA03)

Shen S., Mo H. J., White S. D. M., Blanton M. R., Kauffmann G., Voges W., Brinkmann J., Csabai1 I., 2003, MNRAS, 343, 978

Silva L., De Zotti G., Granato G. L., Maiolino R., Danese L., 2005, MNRAS, 357, 1295

Spergel D. N. et al., 2006, ApJ, submitted (astro-ph/0603449)

Szokoly G. P. et al., 2004, ApJS, 155, 271

Vanzella E. et al., 2005, A&A, 434, 53

Yamauchi C., Gotu T., 2004, MNRAS, 352, 815

Yan L., Thompson D. J., 2003, ApJ, 586, 765

Yan L., Thompson D. J., Soifer B. T., 2004a, AJ, 127, 1274

Yan L. et al., 2004b, ApJS, 154, 75

Zheng W. et al., 2004, ApJS, 155, 73

This paper has been typeset from a TEX/LATEX file prepared by the author.